Hochschule Konstanz
Technik, Wirtschaft und Gestaltung
University of Applied Sciences

EADS DEFENCE & SECURITY

Object Recognition with Surveillance Radar Systems

by

MARTIN KOTHE

Diplomstudiengang Elektro- und Informationstechnik
University of Applied Sciences, Konstanz, Germany

at

EADS Deutschland GmbH
Defence Electronics
Naval Radars

under the supervision of

Dr. rer. nat. DIRK BANKA

Prof. Dr.-Ing. WERNER KLEINHEMPEL

Ulm, July 2008

Declaration

Hiermit versichere ich, dass ich die vorliegende Arbeit selbständig und nur unter Verwendung der angegebenen Quellen und Hilfsmittel verfasst habe. Diese Diplomarbeit wurde bisher in gleicher oder ähnlicher Form keiner anderen Prüfungsbehörde vorlegt.

Ulm, den 10. Juli 2008

Martin Kothe

Abstract

This diploma thesis is devoted to the design and analysis of a radar signal enabling an object classification capability in surveillance radar systems based on high-resolution radar range profiles. It picks up the research results from Kastinger (2006), who investigated classification algorithms for high-resolution radar range profiles, and Meier (2007), who programmed a MATLAB® toolbox for the evaluation of radar signals.

A classical, brief, introduction to radar fundamentals is given (Chapter 1) as well as the motivation for this thesis and certain basic parameters used. After high-resolution radar range profiles are discussed with special focus on surveillance radar systems (Chapter 2), the results of Kastinger (2006) are picked up (Chapter 3) as far as necessary for the following chapters of this thesis.

Following the chapters on radar basics, high-resolution radar range profiles and classification, basic and advanced radar signals are discussed and analysed, especially their range resolution and sidelobe levels (Chapter 4). This includes linear frequency-modulated pulses and nonlinear frequency-modulated pulses as well as phase-coded pulses, coherent trains of identical pulses, and stepped-frequency waveforms. Their analysis is based on Meier's MATLAB® toolbox.

In Chapter 5 we will bring up additional points that have to be considered in radar system design for implementing a classification capability, before this thesis ends with an overall conclusion (Chapter 6).

Zusammenfassung

Diese Diplomarbeit befasst sich mit dem Design und der Analyse von Radarsignalen um die Implementierung einer Klassifikationsbefähigung auf Basis von hochauflösenden Entfernungsprofilen in rundsuchenden Radaren zu ermöglichen. Dabei greift sie die Forschungsergebnisse von Kastinger (2006) und Meier (2007) auf, die sich mit der Klassifikation von hochauflösenden Entfernungsprofilen bzw. mit der Programmierung eines MATLAB® Paketes für die Analyse von Radarsignalen auseinander gesetzt haben.

Zunächst erfolgt eine kurze Einführung in Radargrundlagen, gefolgt von der Motivation für dieses Forschungsthema und einigen grundlegenden Parametern, die in dieser Arbeit verwendet werden (Kapitel 1). Nach einer Einführung in hochauflösende Entfernungsprofile vor dem Hintergrund von Rundsuchradaren (Kapitel 2) werden die Ergebnisse von Kastinger (2006) soweit vorgestellt und zusammengefasst (Kapitel 3), wie es für die weitere Arbeit notwendig ist.

Auf die Kapitel über Radargrundlagen, hochauflösende Entfernungsprofile und Klassifikationsalgorithmen folgt die Analyse einfacher und komplexer Radarsignale mit dem Schwerpunkt auf deren Entfernungsauflösung und Nebenkeulenniveau (Kapitel 4). Dies Umfasst sowohl linear und nichtlinear frequenzmodulierte Pulse als auch phasenkodierte Pulse, kohärente Folgen gleichförmiger Pulse und „frequency-stepped“ Pulsfolgen. Die Analyse erfolgt mit dem MATLAB® Paket von Meier (2007).

In Kapitel 5 werden dann weitere Punkte betrachtet, die Einfluss auf ein Systemdesign mit Klassifikationsbefähigung haben, bevor die Diplomarbeit mit einer abschließenden Zusammenfassung und Bewertung endet (Kapitel 6).

Contents

Acknowledgment

This thesis was written at the Naval Radars section of the Defence Electronics division, at EADS Deutschland GmbH, in Ulm, Germany, and submitted to the Department of Electrical Engineering and Information Technology at the University of Applied Sciences Konstanz, Germany, in partial fulfilment of the requirements for the degree of Diplom-Ingenieur (FH)[1].

First of all, I would like to thank my supervisor at EADS, Dr. Banka, for giving me the opportunity to work in this highly interesting field of research, for providing valuable comments on earlier versions of this thesis, for his support and guidance throughout my work at EADS, and for refocusing my view when necessary.

Furthermore, my thanks go to Mr. Flacke and Mr. Frohwein for their time and the insights they gave me on their ongoing projects, thus providing me with necessary system knowledge, and valuable background information.

Additional thanks goes to my supervisor at the University of Applied Sciences, Prof. Dr. Kleinhempel, for his effort in monitoring the progress of my work. And I also would like to extend my gratitude to EADS Deutschland GmbH for the economic support and to the people of OPES and OPEE, for their advice on many different aspects of this thesis, and the opportunity to discuss my ideas.

Last, but not least, special thanks go to my parents, Bärbel and Gerhard Kothe, for creating a relaxed environment for my studies, for their constant support during the last years, and for believing in me and my abilities.

[1] The professional degree "Diplom-Ingenieur (FH)" is awarded after a four-year-study course including compulsory courses in basic and advanced engineering, specialization courses, and 40 weeks of compulsory practical training. It is concluded by a diploma thesis of four months.

Abbreviations and Acronyms

ACF	Autocorrelation Function
AEWR	Airborne Early Warning Radar
AF	Ambiguity Function
AMTI	Airborne Moving Target Indicator
ARSR	Air Route Surveillance Radar
ASR	Airport Surveillance Radar
CSF	Cross Stepped-Frequency
CW	Continuous Wave
DDS	Direct Digital Synthesizer
DWT	Discrete Wavelet Transform
EM	Electromagnetic
FLOPS	Floating Point Operations per Second
FM	Frequency Modulation
GPR	Ground Penetrating Radar
GUI	Graphical User Interface
HF	High Frequency
HRR	High-Resolution Radar
HPRF	High Pulse Repetition Frequency
IEEE	Institute of Electrical and Electronic Engineering
IF	Intermediate Frequency
IFF	Identification Friend or Foe
ISAR	Inverse-Synthetic-Aperture Radar
JEM	Jet-Engine Modulation
LFM	Linear Frequency Modulation
LO	Local Oscillator
LPA	Linear Power Amplifier
LPRF	Low Pulse Repetition Frequency
MPRF	Medium Pulse Repetition Frequency
NCTR	Non-Cooperative Target Recognition

NLFM	Nonlinear Frequency Modulation
NNA	Nearest-Neighbour Algorithm
PR	Pulsed Radar
PRF	Pulse Repetition Frequency
PRI	Pulse Repetition Interval
RADAR	Radio Detection and Ranging
RBF	Radial Basis Function
RCS	Radar Cross Section
RF	Radio Frequency
RRP	Radar Range Profile
RRM	Rotational Range Migration
RTBS	Radar Target Backscattering Simulation
SAR	Synthetic-Aperture Radar
SCR	Signal-to-Clutter Ratio
SF	Stepped-Frequency
SNR	Signal-to-Noise Ratio
SVM	Support Vector Machine
TRM	Translational Range Migration
UHF	Ultra High Frequency
VHF	Very High Frequency

1 Introduction

1.1 Radio Detection and Ranging

The history of "Radio Detection and Ranging" (*radar*) goes back to the end of the nineteenth / beginning of the twentieth century. In 1904 a patent for the detection of distant metal objects with electric waves was granted to the German Christian Hülsmeyer. But intensive research only began in the 1930s with the aim of using radar techniques for military applications. During World War II, radar technology and systems grew rapidly. In the years following the war, research continued to steadily advance radar capabilities (summary from, e.g., Skolnik (2001)). Since then technologies like Synthetic-Aperture Radar (*SAR*) and many more have been developed and introduced. Today radar also found its way into many non-military applications (e.g., automotive (BMW's ACC®[1])) and research can be expected to continue.

1.1.1 Radar Principle

In principle a radar system emits an electromagnetic (*EM*) wave into free space and "listens" for its echo. If an object is within the radar system's beam, a current is induced, generating an EM-field itself. From this EM-field, called scattering field, an EM-wave is reradiated in all directions.

A small segment of the scattering field is directed back to the radar system. The measured time delay between the transmitted and received wave (T_R), based on two-way propagation, can be used to calculate the range to the object (R) to

$$R = \frac{c \cdot T_R}{2} \tag{1.1}$$

(e.g., Skolnik (2001)), where c denotes the speed of light. For calculations in this thesis c is approximated to $3 \cdot 10^8$m/s.

In modern radar systems however, there are more information available (e.g., position in azimuth (relative to the radar system's antenna), altitude, and/or velocity of the object). Altitude as well as position in azimuth can be obtained form the antenna's physical orientation and/or the beam posi-

[1] ACC® (Active Cruise Control): Active Cruise Control can be programmed to maintain a set speed when the lane ahead is clear, or to reduce speed to keep a safe distance between you and a slower car in front, automatically maintaining that distance until the radar sensors detect that the lane is clear (BMW (2008)).

tion of a phased array antenna. The target's radial velocity can be derived from the Doppler frequency shift (see subsection 1.1.2) of the received wave.

The detection range of a radar system depends on many different factors which are related to each other by the radar equation. A simple form of the radar equation can be derived to

$$R_{max} = \left(\frac{P_{Tx} \cdot A_e^2 \cdot \sigma}{4\pi \cdot \lambda^2 \cdot S_{min}} \right)^{1/4} \tag{1.2}$$

(e.g., Skolnik et al. (2008)), where R_{max} is the maximum detection range of the radar system, P_{Tx} is the transmitted power, A_e is the effective antenna aperture, σ the radar cross section (see subsection 1.1.5 for details), λ is the transmitted wavelength, and S_{min} is the minimal detectable signal.

1.1.2 Doppler Frequency Shift

The difference between the radio frequency (f_0) and the frequency received (f_R) is called Doppler frequency shift (f_d). For $v_R << c$ it is given by

$$f_d = f_R - f_0 = \frac{2 \cdot f_0 \cdot v_R}{c} \tag{1.3}$$

(e.g., Skolnik (2001)), where v_R is the radial velocity of the object relative towards the radar system.

A common agreement throughout the literature is that the Doppler frequency shift has positive values for approaching objects and negative ones for receding objects.

1.1.3 Radar Frequencies

Radar frequencies are separated into radar-frequency bands and letters are used to designate each band. Table 1-1 shows a summary of the letter-band nomenclature that has been officially standardised by the Institute of Electrical and Electronic Engineering (*IEEE*) in IEEE Std 521-2002.

The designations for the radar bands originated from World War II, when secrecy was important. By using the letter reference it was hard to guess what radar band was applied and even harder to get the exact frequency.

Although other letter-band designations exist, i.e., for electronic countermeasures (where the letters A, B, C, etc., are used), IEEE Std 521-2002 states, that they "…are not consistent with radar practice and shall not be used to describe radar-frequency bands." So there may be D-band jammers, but no D-band radar systems.

Band designation	Nominal frequency range	Application(s)
HF	3 – 30MHz	Costal / Over-the-horizon surveillance
VHF	30 – 300MHz	Long-range air surveillance
UHF	300 – 1000MHz	Long-range air surveillance (e.g., Airborne Early Warning Radar (*AEWR*)); Ground Penetrating Radar (*GPR*)
L	1 – 2GHz	Long-range air surveillance (e.g., Air-Route-Surveillance Radar (*ARSR*))
S	2 – 4GHz	Medium-range surveillance (e.g., Airport-Surveillance Radar (*ASR*)); Long-range weather
C	4 – 8GHz	Medium-range surveillance; Long-range tracking
X	8 – 12GHz	Short-range tracking; Imaging; Missile guidance
K_u	12 – 18GHz	High-resolution mapping
K	18 – 27GHz	Weather (e.g., rain cloud detection)
K_a	27 – 40GHz	Very high-resolution mapping; Airport-surveillance
V	40 – 75GHz	
W	75 – 110GHz	Automotive
mm	110 – 300GHz	

Table 1-1 Letter Designations for Radar-Frequency Bands (IEEE Std 521-2002)

1.1.4 Radar Systems

Radar systems have been developed for many different applications (e.g., in Table 1-1). So they can be classified based on their functionality. According to Skolnik (2001) another way of classifying radar systems is based on the signals they utilize.

Continuous Wave (*CW*) radar systems continuously emit an EM-wave and use separate transmit and receive antennas. Their main applications are velocity measurement (e.g., police radar speed gun) and object tracking.

Pulsed Radar (*PR*) systems transmit their signals in form of trains of pulses. So Eq. (1.1) can be used to obtain range information. A single pulse is of the width τ_P and the time between two following pulses is T_P, which is often also referred to as the Pulse Repetition Interval (*PRI*). The inverse of the PRI is the Pulse Repetition Frequency (*PRF*),

$$PRF = \frac{1}{PRI} = \frac{1}{T_P} \tag{1.4}$$

If the PRF is too high, an echo from a long-range object might arrive after the transmission of and be mistakenly associated with the next pulse. These multiple-time-around echoes can result in an ambiguous range measurement. If the PRF is too low, range ambiguities can be avoided, but therefore ambiguous Doppler (velocity) measurements occur. Systems with a low PRF (*LPRF*) are primarily used for ranging, whereas a high PRF (*HPRF*) is used to measure object velocity. A medium PRF (*MPRF*) suffers from both, range and Doppler ambiguities.

1.1.5 Radar Cross Section

As described by Knott et al. (1993), the Radar Cross Section (*RCS*) is a measure of the backscattered energy from an object compared to the received energy at the radar system, "standardized" to an infinite distance. So if the distance between the radar system and the object is large enough that one can assume the waves scattered by the object and received by the radar system to be spherical, the RCS can be expressed by

$$\sigma = \lim_{R\to\infty} \; 4\pi R^2 \frac{|E_s|^2}{|E_i|^2} \tag{1.5}$$

where R is the distance between the radar system and the object, E_i is the electric field strength of the incident wave and E_s of the scattered wave.

As we can see, the unit of the RCS is square meters. But the RCS does not represent the physical size of the backscattering object. Instead the RCS given in Eq. (1.5) is a representation of a metal sphere that would scatter the same energy in the same direction as the observed object does. The RCS depends heavily on the structure and material of the object, the radar frequency and polarization, and the aspect angle (see section 2.2).

1.1.6 Radar Range profile

If the object of interest is a single dimensionless point scatterer, as assumed in subsection 1.1.5, we can associate its backscattered energy with a certain range using Eq. (1.2). A radar range profile (or simply range profile) is a plot of the backscattered energy from an object versus its range. Radar range profiles will be discussed in more detail in chapter 2.

1.1.7 Range Resolution

Following Wehner (1995), the radar system's ability to detect objects in close proximity to each other as distinct objects is described by the radar system's range resolution (ΔR), given by

$$\Delta R = \frac{c \cdot \tau_P}{2} = \frac{c}{2 \cdot B} \tag{1.6}$$

where B is the bandwidth. The equality of $\tau_P = 1/B$ (for an unmodulated signal) results from the Rayleigh criterion and is shown in detail in, e.g., Wehner (1995).

From Eq. (1.6) it follows, that a higher range resolution can be achieved by either decreasing the pulse width or increasing the bandwidth. For an unmodulated signal a decrease in τ_P is equal to a decrease in transmitted energy. But following Eq. (1.2) decreased transmitted energy leads to a

decreased maximum detection range. So a higher range resolution has to be paid for by a lower maximum detection range. How this undesirable conflict in radar system design can be solved will be discussed in chapter 4.

1.1.8 Clutter

Skolnik (2001) defines clutter as "…the term used by radar engineers to denote unwanted echoes from the natural environment." Depending on the RF, clutter can include natural echoes, i.e., from ground, sea, weather, birds, ionized meteor trails, or aurora. But also unwanted backscattering from artificial objects is considered as clutter (e.g., windmills, television towers, chaff[2]).

What undesirable echoes are depends on the application of the radar system. For a weather radar system, backscatter from rain clouds might be of high interest and therefore not to be considered as clutter. Another example would be backscatter from land that might be seen as clutter for an ARSR but for a ground-mapping radar system might be the prime object of interest.

1.2 Motivation

On the 3rd July 1988 an Iranian passenger jet (Flight IR655) was shot down in the Persian Gulf by a SM-2[3] from the Aegis system of the naval warship USS Vincennes. All 290 passengers aboard the Airbus A300 died. The crew of the USS Vincennes erroneously believed they were firing at an Iranian F-14 fighter aircraft (BBC News (www1)).

Most of today's aircraft are equipped with a system for Identification Friend or Foe (*IFF*). IFF is based on a challenge-response-principle and therefore depends on the object's cooperation for correct identification. But the process of identification can return incorrect results either by deliberately transmitted false responses or because of technical incapability (i.e., wrong encryption, jamming, overloaded transponder, etc.), leading to tragic incidents like in case of Flight IR655.

To further reduce the uncertainty in IFF, without having to resort to visual confirmation, research on techniques for Non-Cooperative Target Recognition (*NCTR*) is performed. The idea behind this approach is that the geometry of or moving parts on an object impose features in a reflected radar signal that are characteristic of the object and may therefore be used for classification. Radar range profiles can be interpreted as a one-dimensional representation of an object's geometry.

Three NCTR techniques were compared by van der Heiden (1998). From this it is taken, that High-Resolution Radar (*HRR*) range profiles only need a relatively short time on target, compared

[2] Chaff is an electronic countermeasure that consists of a large number of thin passive reflectors. When released from an aircraft they are dispersed by the wind to form a highly reflecting cloud.
[3] SM-2 (Standard Missile-2): SM-2's primary role is to provide area defence against enemy aircraft and anti-ship cruise missiles (Raytheon (www1)). It is produced by Raytheon Company.

to Inverse-Synthetic-Aperture Radar (*ISAR*), and are not as heavily dependent on aspect angle for data acquisition as, i.e., the Jet-Engine Modulation (*JEM*). For 360-degree surveillance radar systems, as presumed in this thesis (for system parameters see section 1.3), the time on target was the most important criterion for selecting HRR range profiles as classification approach.

1.3 System Parameters

All considerations and simulations in this thesis are based on a radar system which is presumed to have the following parameters:

Parameter	Value	Comment
Radar Type	360° Surveillance	Possible targets: e.g., aircraft, helicopter, small sea vessels, guided missiles
Scan rate	2s	
Number of Burst Forms	2	one LPRF & one MPRF burst
Baseband Frequency Band	'VHF'	
Intermediate Frequency Band	'L'	
Frequency Band	'C'	
Available Radar Bandwidth	> 400MHz	
Beam width	1.6°	
Burst Repetition Interval	10ms	
LPRF Burst		
Range of Interest	30km	
Signal Bandwidth	30MHz	
Burst length	3ms	
Pulses per Burst	8	
Pulse Repetition Interval	375µs	
Pulse Width	2µs	
MPRF Burst		
Range of Interest	200km	
Signal Bandwidth	7.5MHz	
Burst length	6.4ms	
Pulses per Burst	32	
Pulse Repetition Interval	200µs	
Pulse Width	20µs	

Table 1-2 System Parameters used within this Thesis

2 Radar Range Profiles

2.1 Introduction

A Radar Range Profile (*RRP*) is a one-dimensional representation of an object's geometry. It is the projection of the backscattered energy from an object onto the radar system's line-of-sight. A basic description of the process of generating RRPs is provided by Wehner (1995). If the radar signal utilized provides for sufficient range resolution (see subsection 1.1.7), it is possible to resolve different scattering centres, thus providing information on the geometry (see Figure 2-1) and making HRR range profiles suitable for NCTR (i.e., shown by van der Heiden and de Vries (1996)).

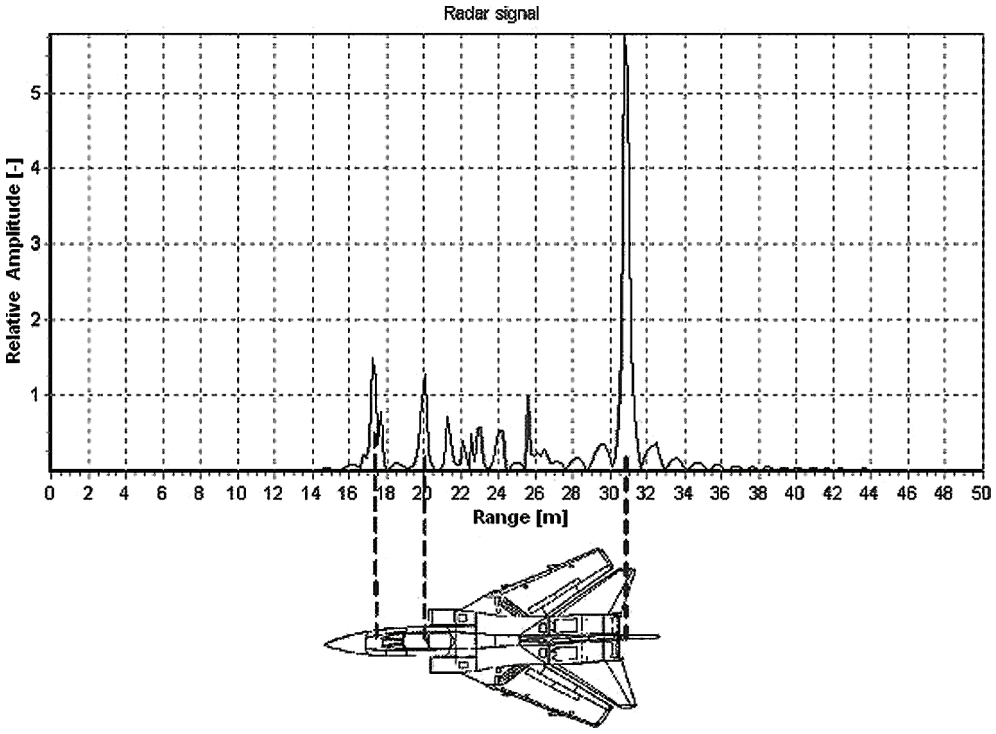

Figure 2-1 Radar Range Profile of a Tornado as simulated by Kastinger (2006)

This chapter will give an introduction to radar range profiles. After basic definitions in section 2.2, sources of range profile variability will be presented in section 2.3. How range profiles can be improved by pre-processing is part of section 2.4, and the chapter will be closed by a summary in section 2.5.

2.2 Definitions

The position of an object in relation to a radar system can be determined by the radar system's antenna azimuth and elevation in combination with the measured distance from Eq. (1.1).

A single object can change its orientation by rotating about an arbitrary axis. This rotation can be decomposed into roll, yaw, and pitch motions (illustrated by Figure 2-2).

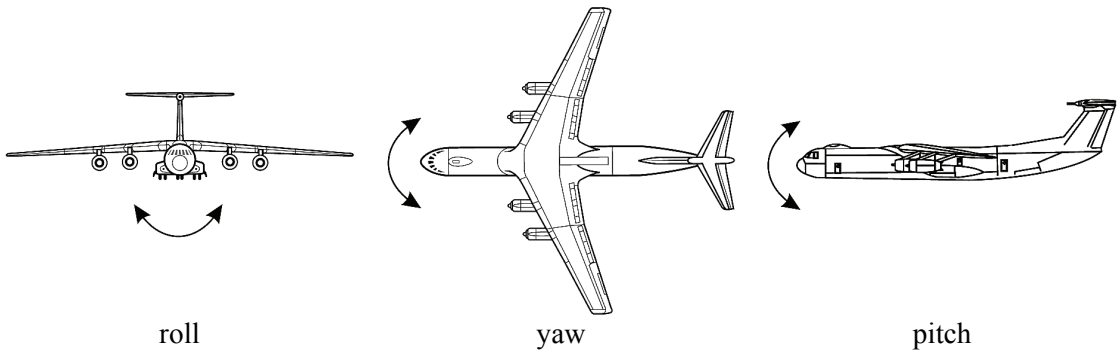

Figure 2-2 Three Basic Rotational Motions (from van der Heiden (1998))

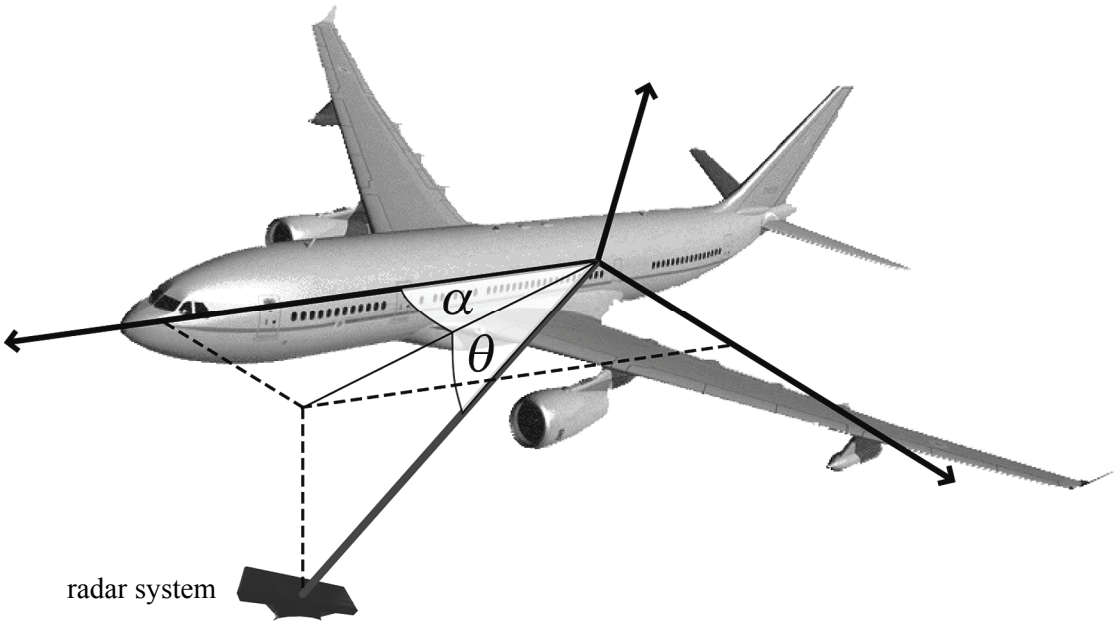

Figure 2-3 Definition of Aspect Angle

The superposition of relative position and object orientation can be expressed as target aspect angle. According to van der Heiden (1998) the target aspect angle is a coordinate pair with two components: aspect azimuth α and aspect elevation θ. The aspect azimuth α is defined as the angle

between the direction of the nose of the aircraft and the direction of the radar system's line-of-sight projected on a plane through the aircraft's nose and wingtips. The aspect elevation θ is defined as the angle between the radar system's line-of-sight and the plane through the aircraft's nose and wingtips (see Figure 2-3). Note that if the aircraft flies with zero roll and zero pitch angle the aspect elevation equals the radar system's elevation.

Changes in target aspect angle are a major source for fluctuations and variability in RRPs (see section 2.3 and Figure 2-4).

2.3 Variability

In this section we will follow Zwart (2003), who lists five different sources for range profile variability: measurement noise, translational range migration, rotational range migration, speckle, and occlusion.

2.3.1 Measurement Noise

All radar systems are affected by measurement noise. The two main sources of measurement noise are thermal noise in the radar system's receiver and clutter (see subsection 1.1.8).

2.3.2 Translational Range Migration

A change in distance between object and radar system causes scatterers to move to an adjacent range bin. This is called Translational Range Migration (*TRM*). As all scatterers are translated by the same amount, no change in relative distance between single scatterers takes place. So TRM does not influence the shape of the range profile, but is responsible for a translation of the original range profile.

2.3.3 Rotational Range Migration

If an object rotates over an azimuth angle of a few degrees, such that the outermost scatterers move from one range bin to an adjacent one, the range profiles measured during this rotation suffer from Rotational Range Migration (*RRM*). The same effect occurs if the aspect elevation changes over an angle in the same order of magnitude.

2.3.4 Speckle

In addition to RRM, a rotating object will also cause speckle. If in a single range bin two or more distinct scatterers are present, a slight change in aspect angle (azimuth or elevation) can change their differential distance to the radar system over half the wavelength. This causes the coherent

sum of the scatterers' contributions to turn from constructive to destructive interference (or vice versa). The change in aspect angle is due mainly to small yaw motions during measurement. Speckle occurs for changes in aspect angle which are one to two orders of magnitude smaller then for RRM. In a sequence of consecutively measured range profiles speckle will cause the amplitudes to vary rapidly.

2.3.5 Occlusion

Occlusion describes the effect, that not always all scatterers on an object are observable by the radar system. The object's geometry, aspect angle, and change in aspect angle contribute to this effect causing variations in the range profile amplitudes.

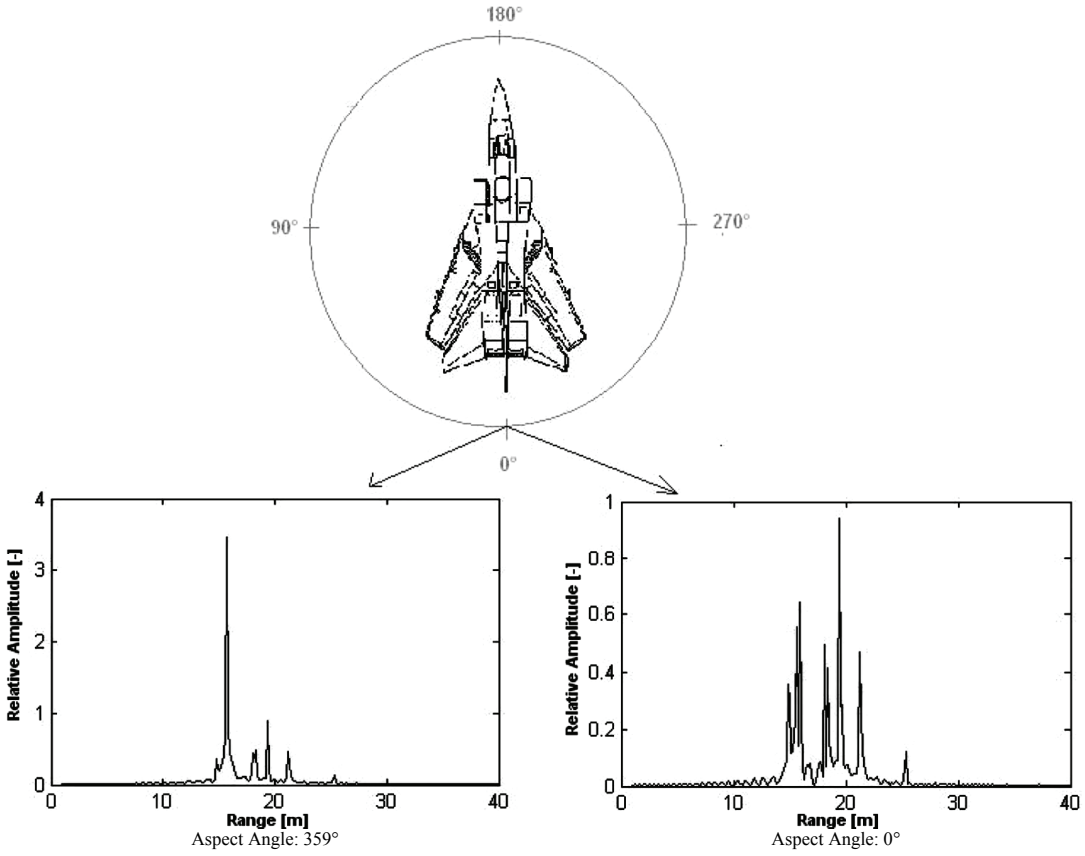

Figure 2-4 Range Profiles Variability due to Small Changes in Aspect Angle (from Kastinger (2006))

2.4 Influence of Pre-processing

While the range resolution (see subsection 1.1.7) of radar range profiles can be improved by utilizing a signal either with a small pulse width or a large bandwidth, there are other aspects that have to be considered concerning the detection of objects.

If a signal with a set bandwidth B is used, this is similar to applying a rectangular shaped window to the signal in the frequency domain, which then introduces relatively strong sidelobes in the range domain (e.g., Levanon and Mozeson (2004)). The undesired effect of high sidelobes is the masking of weak signals returned from other objects. To reduce sidelobe levels it is common to introduce a filter in the radar system's receive path. There is a large choice in filters available, an overview of which was given by Harris (1978). Each filter has advantages and disadvantages. Levanon and Mozeson (2004) showed, i.e., that a Hamming weight window can reduce the time sidelobes to approximately -40dB compared to -13.2dB of an unweighted signal (see Figure 2-5). From the comparison it is also visible, that the Hamming window increases the nominal range resolution by roughly the factor 1.3. So for a Hamming window Eq. (1.6) can be rewritten to

$$\Delta R_{Hamming} \approx 1.3 \cdot \Delta R = 1.3 \frac{c}{2 \cdot B} \tag{2.1}$$

Other techniques (i.e., used by van der Heiden (1998) or Zwart (2003)) for improving RRPs through pre-processing are zero-padding before applying the discrete Fourier transform (thus allowing for easier amplitude peak detection), and other algorithms to convert the raw measurement data to another number space, making it more suitable for a certain classifier (see chapter 3). During pre-processing compensation for TRM is also possible.

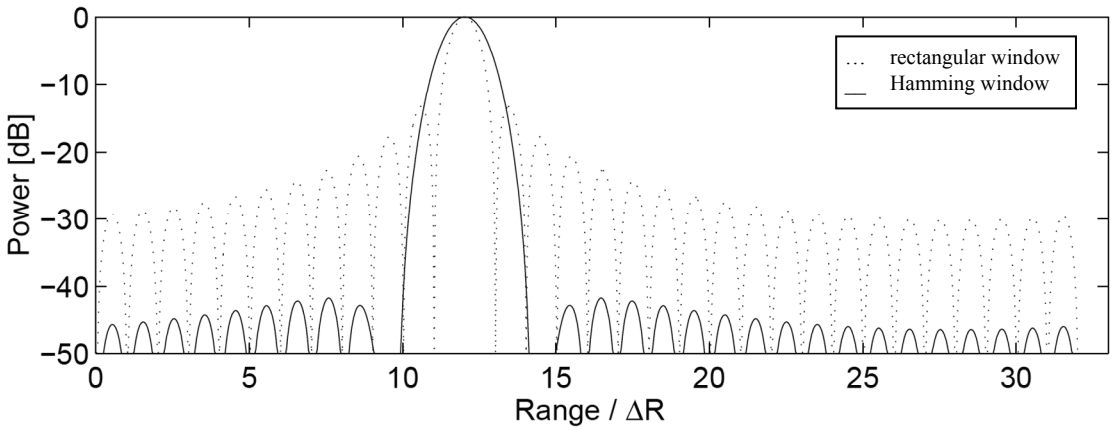

Figure 2-5 Sidelobe Levels for Rectangular and Hamming Window

2.5 Summary

In this chapter radar range profiles were introduced as an approach for NCTR, as they provide information on an object's geometry. Then, the target aspect angle was defined to describe an object's position and orientation towards a radar system. Based on five effects that can influence range pro-

files, target aspect angle was then presented as the major source for radar range profiles variability. Finally, pre-processing techniques and their influence on radar range profiles were introduced.

3 Classification using Radar Range Profiles

3.1 Introduction

Classification is performed by classifiers. So a classifier is an integral part of a NCTR system. It has to assign object data of unknown origin to a specific type within a database.

In many cases a classification problem is a pattern recognition problem, as is the case for radar range profiles. The topic of pattern recognition is still a wide area of research, and although many techniques are available, only a limited number of pattern recognition techniques can be applied here, due to some limiting properties (e.g., variability (see section 2.3)) of range profiles.

The five general components of a pattern recognition system are shown in Figure 3-1. The sensor could be, i.e., a radar system. During segmentation gathered raw data is separated into individual patterns. The feature extractor reduces the raw data so an object can be recognized by measurements whose values are very different for objects in different categories. These values are stored in a feature vector which is then used by the classifier to assign the object to a category. Finally in post-processing the output of the classifier is used to decide on a recommended action. With certain classifiers, it is possible to skip feature extraction.

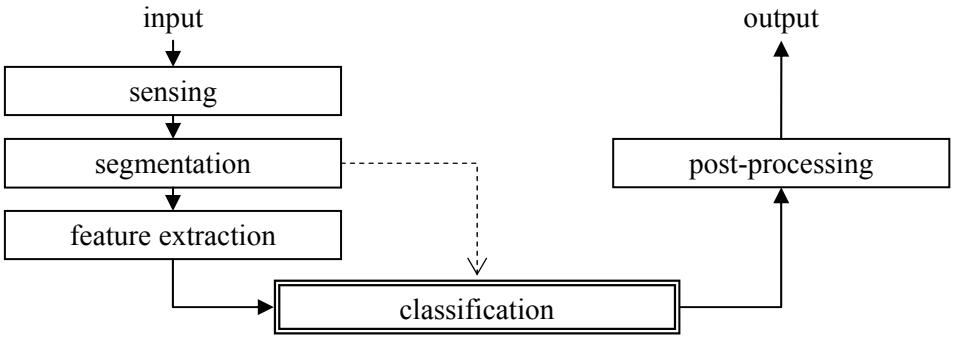

Figure 3-1 Components of a Pattern Recognition System (Duda et al. (2001))

In the next four sections (3.2 to 3.5) four classifiers will be presented, including their performance[1] and accuracy[2]. A summary in section 3.6 will close this chapter.

[1] Less time needed for a decision from a given test set is associated with a better performance of the classifier.
[2] The lower the over-all error on a given test set the higher is the accuracy of the classifier.

3.2 Bayesian Decision Theory

A fundamental statistical approach to a pattern recognition problem is the Bayesian decision theory. As explained in Duda et al. (2001) it is based on classification decisions and their probabilities. It requires that the problem can be fully posed in probabilistic terms and it implies that all relevant probabilities have to be known a priori.

In a scenario where two different types of objects enter an area of interest and we should predict which type will enter next, we need certain knowledge to achieve a low over-all error. In a first step the probabilities of appearance for both types are described and denoted as $P(m_i)$. To improve the prediction, we have to include a more specific knowledge. The features (for aircraft, i.e., a RRP) of each type will be stored in a feature vector $\mathbf{x}$. The combination of prior knowledge and feature vector describes how likely it is to find a pattern of type m having feature values $\mathbf{x}$. This connection is expressed by the Bayes formula (e.g., Duda et al. (2001)):

$$P(m_i \mid \mathbf{x}) = \frac{p(\mathbf{x} \mid m_i)P(m_i)}{p(\mathbf{x})} \tag{3.1}$$

where, in case of our example with two types,

$$p(\mathbf{x}) = \sum_{i=1}^{2} p(\mathbf{x} \mid m_i)P(m_i) \tag{3.2}$$

and $P(m_i|\mathbf{x})$ denotes the a posteriori probability – the probability of the object entering the area being of type m given that the feature vector $\mathbf{x}$ has been measured.

For a decision the Bayesian classifier has to compute a discriminant function for all categories for each $\mathbf{x}$. So the computational effort increases linearly with the number of categories. According to van der Heiden (1998) its sensitivity towards RRM has to be taken into account, too. So an effort has to be made to implement a very accurate aspect angle estimation. In Kastinger (2006) based on eight categories the classifier needed 150ms for one decision.

In the same simulations the Bayesian classifier produced an over-all error of 81% based on five categories of simulated RRPs and 49% based on three categories of measured RRPs. It is also taken from there that the SNR is the limiting factor for the accuracy of this classifier.

3.3 Nearest-Neighbour Algorithm

The Nearest-Neighbour Algorithm (*NNA*) assigns objects to categories based on geometric similarity. So if we have a set $D^n=\{\mathbf{x}_1,\ldots,\mathbf{x}_n\}$ of n labelled prototypes from which $\mathbf{x}'\in D^n$ is the prototype

nearest to a test sample **x**, then the NNA would assign **x** the label associated with **x′**. In Figure 3-2 a) this means **x** would be assigned the label associated with the bolded red dot (Duda et al. (2001)).

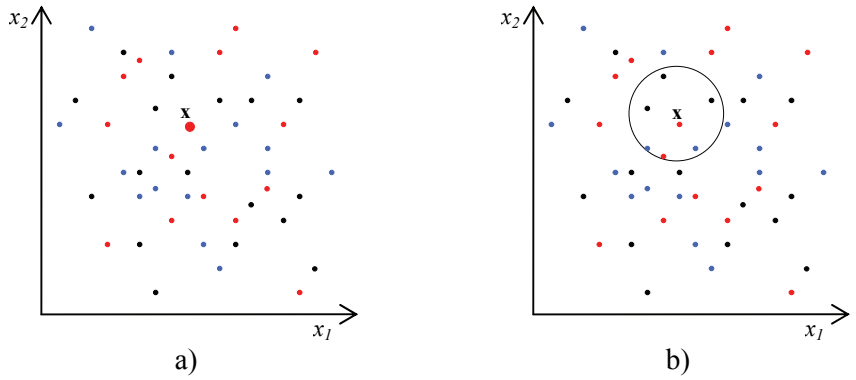

Figure 3-2 Example for a) Nearest-Neighbour Rule and b) 7-Nearest-Neighbour Rule

An extension of the NNA is the k-nearest-neighbour algorithm. As the name implies, this algorithm assigns **x** the label associated with the category most frequently represented among its *k* nearest neighbours. Figure 3-2 b) shows this approach for k=7, where **x** would be assigned the label associated with the category of the black dots.

The problem of the k-NNAs is the large computational costs, which increase linearly with the number of prototypes as the distances to all prototypes in D^n for each **x** have to be computed. In simulations by Kastinger (2006) the decision time of the NNA based on eight categories was 1-2s.

For the accuracy of the NNA Kastinger (2006) gives an over-all error of 51% based on eight categories of simulated RRPs and 48% based on three categories of measured RRPs. Based on five categories of measured RRPs van der Heiden (1998) gives an over-all error of 24%.

3.4 Radial Basis Functions

Radial Basis Functions (*RBF*s) provide a way to construct a function that maps vectors from a high dimensional space onto a lower dimensional space (Broomhead and Lowe (1988)). Like the NNA, RBFs use the geometric distance between range profiles for a decision. The advantage of RBFs implementations compared to the NNAs is that it generalizes the training data, thus providing for a far more efficient classifier in terms of memory use and classification speed. More information on RBFs for range profile classification can be found, i.e., in van der Heiden (1998).

The classification effort in van der Heiden (1998) is gives in floating point operations per second (*flops*). It was shown that, based on a training set of 120 range profiles, the RBFs are 5 to 6 times faster then a NNA.

Based on the same training set of 120 measured range profiles, van der Heiden (1998) gives an over-all error for RBFs of 13%.

3.5 Support Vector Machines

Support Vector Machines (*SVM*s) are nonlinear generalized, practical implementations of the generalized portrait algorithm presented by Vapnik and Lerner (1963). They have been proven to be applicable to pattern recognition problems, i.e., for text categorization (Joachims (1997)) or object recognition (Blanz et al. (1996)). Today, SVMs are an active area of research.

A SVM is a type of kernel[3] machine using pre-processed data to represent features in a higher dimension. With an appropriate nonlinear mapping to sufficiently high dimension, data from two categories can be separated by a hyperplane (Duda et al. (2001)). The benefit of this mapping is that nonlinear class distribution boundaries in the domain space can become linear in the feature space (see Figure 3-3).

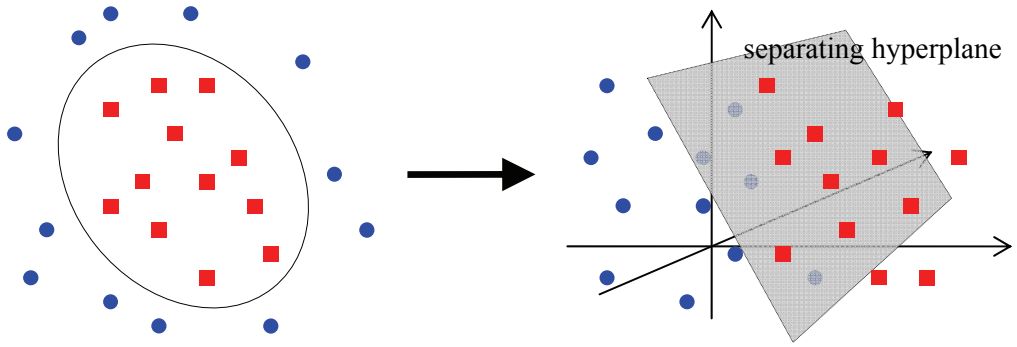

Figure 3-3 Nonlinear Mapping for Easier Separation (from Markowetz (2003))

SVMs were originally developed for the linear separation of two-class-problems (Schölkopf and Smola (2001)). But often a linear separation is not possible for complex real world applications. To solve this problem the use of multiple layers of linear threshold functions was proposed which led, i.e., to the development of multilayer neural networks[4]. In the newer research on SVMs extensions have been introduced to overcome the original limitation to linear separable two-class-problems (e.g., soft-margin functions).

Depending on what multi-class-approach is taken, the decision time of the classifier varies considerably. For the one-against-all approach on eight categories, Kastinger (2006) measured a deci-

[3] A set of functions providing nonlinear transformations is called a kernel.
[4] For an introduction to neural networks and their performance in range profile classification see Kastinger (2006). A more general description of neural networks for pattern classification can be found, i.e., in Duda et al. (2001).

sion time of 2.5s. He also showed, that this time could be reduced using pre-processing techniques (e.g., wavelet compression), while, i.e., Tsujinishi et al. (2004) have shown that a pair wise multi-class-approach has better decision times then one-against-all or all-at-once.

For the accuracy of SVMs Kastinger (2006) gives an over-all error of 32% based on eight categories of simulated RRPs and 36% based on three categories of measured RRPs.

3.5.1 Wavelet Transform

The continues wavelet transform is a method to convert a time signal into another representation (time-frequency) without any loss of information (Mallat (1999)). A fast and efficient implementation of it is the Discrete Wavelet Transform (*DWT*) algorithm.

Kastinger (2006) investigated the influence of the DWT on the classification of range profiles. He showed that different decomposition[5] levels can be compared to different signal bandwidths utilized. For SVMs, the use of the DWT in pre-processing reduced the decision time (incl. processing time) for a one-against-all approach with eight categories from 2.5s to ~510ms. As for the accuracy, with decomposition level 5 the over-all error for three categories of measured RRPs increased to 42% while level 3 decreased the over-all error to 34%.

Other then Unterberg (2005), who argued that optimal classification results require a high bandwidth (B > 800MHz), based on his simulations Kastinger (2006) showed that a signal bandwidth of ~200Mhz leads to optimal classification results for objects of about 20m in size.

3.6 Summary

After a brief introduction to pattern recognition systems four different classifiers have been introduced. While all introduced classifiers are suitable for classification of radar range profiles in general, they show very different results in performance and accuracy. While the probability based Bayesian decision theory is the fastest classifier introduced, it also showed the poorest accuracy. The k-NNAs showed a better accuracy but also the poorest performance of all introduced classifiers. Thereafter RBFs were presented in short, as they have been used for range profile classification in live measurement campaigns. Finally SVMs, which have poor performance but achieve good accuracy, were discussed and the DWT was presented as a possibility to further improve performance and accuracy in classification of radar range profiles.

[5] With each decomposition step, information is removed and the signal dimension is halved. This low-pass filtering leads to a reduction in range resolution but also to a reduction in noise.

Classifier	Performance[6]	Accuracy[7]	Comment
Bayesian Decision Theory	150ms	51%	very sensitive to all sources of range profile variability
Nearest-Neighbour-Algorithm	1-2s	52%	very sensitive to RRM, speckle and occlusion
Radial Basis Functions[8]	170-340ms	87%	
Support Vector Machines	2.5s	64%	
Support Vector Machines, DWT[9]	~510ms	66%	use of decompression levels improves SNR

Table 3-1 Summary of Classifier Results on Radar Range Profiles

[6] Performance based on one decision from a test set of eight categories.
[7] Accuracy based on a test set of three measured RRPs.
[8] For the RBFs only evaluation of measured data from van der Heiden (1998) is available, who's data cannot be compared directly to Kastinger (2006).
[9] Decomposition level 3

4 High Resolution Radar Signals

4.1 Introduction

For the design of a pulsed radar system there exist many conflicting requirements. Two of them normally are the desired maximum detection range and the desired range resolution. In the early stages of radar development these two requirements mend that the waveform design had to be a compromise on the pulse width τ_P – wide enough to provide for an acceptable maximum detection range and narrow enough for good range resolution (Cook and Bernfeld (1967)).

It has been Woodward (1953), who introduced the idea that the transmitted pulse could be designed to meet the detectability requirement and after that could be modulated to satisfy the range resolution requirement. He pointed out that range resolution and accuracy are functions of the signal bandwidth, and not of the transmitted pulse width.

According to Levanon and Mozeson (2004) a signal's waveform is responsible for the accuracy, resolution, and ambiguity of determining the range and radial velocity (also referred to as range rate) of an object. While the range is related to the delay of the received signal by Eq. (1.1), range rate is associated with the Doppler Frequency Shift of the signal received.

In the following the matched filter (subsection 4.1.1) and a tool for the analysis of its output, the ambiguity function (subsections 4.1.2 and 4.1.3), will be introduced. In section 4.2 modulated and in section 4.3 coded single pulses are investigated, followed by a coherent train of identical pulses in section 4.4. Finally, stepped-frequency waveforms will be presented (section 4.5), before our conclusions (section 4.6) end this chapter.

4.1.1 Matched Filter

In radar systems the received signal is passed through a filter which is matched to signal. The output peak (also called mainlobe) of this matched filter[1] will be a function only of the signal's energy. The waveform only has an influence on the output before and after the peak (also called sidelobes). If the time sidelobes remain too high over an extended delay this results in uncertainty as to which is the true delay (range). From the output of the matched filter the resolution performance of the

[1] The concept of a matched filter is discussed in much more detail in, i.e., Cook and Bernfeld (1967), Wehner (1995), Ludloff (2002), Skolnik (2001) or Levanon and Mozeson (2004).

signal can be determined. It is the width of the mainlobe, measured at its -3dB point. To measure the radial velocity a radar system's receiver incorporates a filter bank where each filter is matched to a predefined Doppler-shifted version of the signal. As for delay, a narrow output for Doppler should be achieved so that objects at different velocities cause peaks at different Doppler-shifted matched filters (Levanon and Mozeson (2004)).

The tool for studying the two-dimensional response (in delay τ and Doppler f_d) of a matched filter is the ambiguity function.

4.1.2 Ambiguity Function

Based on his definition of a correlation function $\chi(\tau,\vartheta)$ as

$$\chi(\tau,\vartheta) = \int u(t)u^*(t+\tau)\exp(-2\pi j\,\vartheta)dt \tag{4.1}$$

Woodward (1953) introduced the squared magnitude of this function as the ambiguity diagram which became commonly referred to as the Ambiguity Function (*AF*). But his definition of ϑ was not clear, so that Sinsky and Wang (1974) proposed a standardized definition of the radar ambiguity function. Their definition was picked up by the IEEE and IEEE Std 686-2008 states:

> "**ambiguity function**: The squared magnitude $|\chi(\tau,f_d)|^2$ of the function that describes the response of a radar receiver to point targets displaced in range delay (τ) and Doppler frequency (f_d) from a reference position, where $|\chi(0,0)|$ is normalized to unity. … The ambiguity function is used to examine the suitability of radar waveforms for achieving accuracy, resolution, freedom from ambiguities, and reduction of unwanted clutter." [2]

This is expressed mathematically by

$$\left|\chi(\tau,f_d)\right|^2 = \left|\int u(t)u^*(t+\tau)\exp(2\pi j f_d t)dt\right|^2 \tag{4.2}$$

where $u(t)$ is the transmitted waveform, suitably normalized, and $u^*(t)$ is the complex conjugate of $u(t)$ while positive τ indicates an object beyond the reference delay and positive f_d indicates an approaching object.

The AF has four main properties. Prove of these properties can be found in, i.e., Levanon and Mozeson (2004).

(1) Maximum at (0,0): The AF can nowhere be higher than at the origin.

$$\left|\chi(\tau,f_d)\right|^2 \le \left|\chi(0,0)\right|^2 = 1 \tag{4.3}$$

[2] Though not consistent with IEEE Std 686-2008, the definition of the ambiguity function as $|\chi(\tau,f_d)|$ can still be found in radar literature (e.g., Levanon and Mozeson (2004)).

(2) Constant volume: The total volume under the AF is independent of the signal waveform and equals unity.

$$\iint \left|\chi(\tau, f_d)\right|^2 d\tau \; df_d = 1 \tag{4.4}$$

(3) Symmetry with respect to the origin:

$$\left|\chi(\tau, f_d)\right|^2 = \left|\chi(-\tau, -f_d)\right|^2 \tag{4.5}$$

(4) Linear FM effect: Using linear frequency modulation (see section 4.2.1) as signal waveform shears the resulting AF which introduces range-doppler coupling.

$$u(t)\exp\left(j\pi k t^2\right) \Leftrightarrow \left|\chi(\tau, f_d - k\tau)\right|^2 \tag{4.6}$$

Range-doppler coupling, as explained by Skolnik et al. (2008), causes the output peak of the matched filter to be shifted in time proportional to the Doppler frequency shift. It occurs earlier in time for a target with a positive Doppler frequency shift compared to a stationary target at the same range, assuming a positive linear modulation slope and later in time for a negative slope.

4.1.3 MATLAB® toolbox

For the evaluation of signal waveforms in this thesis the MATLAB® toolbox[3] from Meier (2007) was available. The toolbox includes three components: signal generator, matched filter, and evaluation (see Figure 4-1). The matched filter computes the response to a given signal waveform. This signal can be a time row generated by the signal generator based on user defined input parameters or a time row of amplitude values read directly from an ASCII-file. The matched filter output can be evaluated as to, i.e., sidelobe levels, resolution or Doppler.

Meier (2007) verified the output of the toolbox's matched filter using simple, well-known signals (e.g., linear frequency-modulated pulse (see subsection 4.2.1) or binary phase-coded pulse (see subsection 4.3.1)) and compared it to the research results published by Mahafza (2005), Rihaczek (1996) or Skolnik (2001). The focus for the parameters of the signals used for verification was on relatively measured values, i.e., the time-bandwidth product of the signal. However, using the parameters assumed in section 1.3 the evaluation of a single linear frequency-modulated pulse (τ_P=2µs, T_P=375µs, f_0=5.4GHz, B=30MHz) on the workstation[4] available resulted in a MATLAB® "Out of Memory"-error.

[3] Source code comes on CD-ROM with this thesis.
[4] HP Compaq Business PC dc7600 Convertible Minitower (Intel Pentium 4 HT 3.0GHz, 512MB RAM, 80GB SATA HDD, Microsoft Windows XP Professional (32-bit), MATLAB® 7.0.1, MATLAB® R2007a)

In a first step all Graphical User Interface (*GUI*) elements were disabled reducing the calculation time by factor 1.5 but not having any influence on the memory utilization. In a second step the MATLAB® code was rewritten to optimize memory utilization by reducing loop structures, reducing the data stored in workspace during calculations, disabling plots, replacing the automatic sampling (T_S) rate by a constant one (equal to the sampling rate used for signal patterns in the radar system's Direct Digital Synthesizer (*DDS*), T_S=16.6ns), and, as the duration of the signal increases, reducing the number of samples used for calculating Doppler frequency domain. In the last step the calculations were performed on Microsoft Windows XP Professional with the "3GB"-switch enabled (by that allocating additional 1GB of virtual address space to processes) as described in Mathworks (2008) and running MATLAB® without GUI (calling MATLAB® from the command prompt using the "No Java Virtual Machine"-switch ("`matlab.exe -nojvm`")). For additional information on "Out of Memory"-errors and the MATLAB® memory management in general also see Mathworks (2008) and its referring documents.

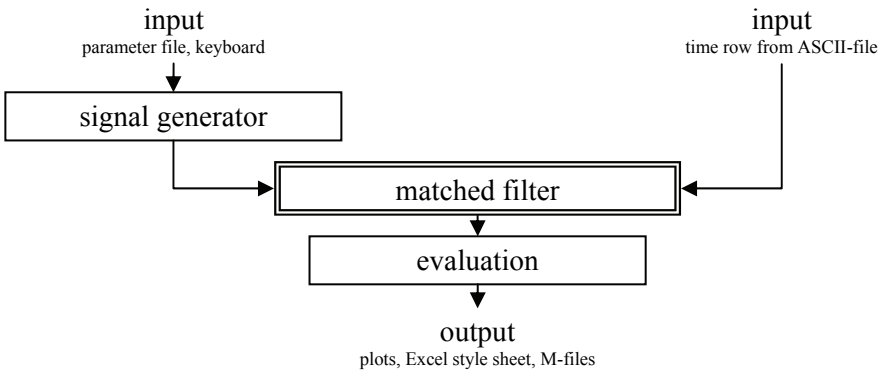

Figure 4-1 Components of the MATLAB® toolbox from Meier (2007)

With these optimizations it was possible to evaluate the range delay performance of baseband signals up to a single LPRF burst (see section 1.3 for detailed parameters). Due to the decreased number of samples for Doppler frequency for longer pulse trains the evaluation of their Doppler performance was only possible for single pulses.

4.2 Frequency-modulated Pulses

4.2.1 Linear Frequency Modulation

The Linear Frequency Modulation (*LFM*), or chirp, was the first and probably still is the most popular modulation/code for achieving a high signal bandwidth without a decrease in maximum detection range. The idea behind LFM is to sweep a frequency band of bandwidth *B* linearly for the

pulse duration (T) (see Figure 4-2) resulting in a time-bandwidth product (BT) larger then that of an unmodulated pulse (BT=1).

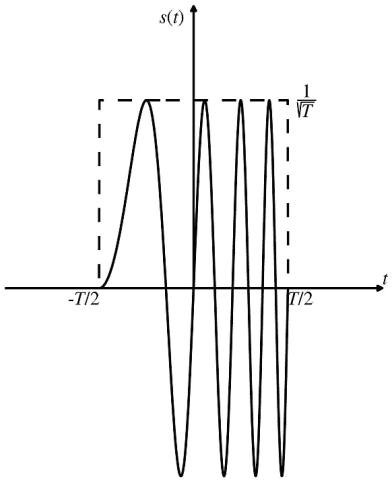

Figure 4-2 Linear Frequency-modulated Pulse (from Levanon and Mozeson (2004))

A LFM pulse is represented by its complex envelop

$$u(t) = \frac{1}{\sqrt{T}} \text{rect}\left(\frac{t}{T}\right) \exp\left(j\pi k t^2\right) \tag{4.7}$$

(e.g., Levanon and Mozeson (2004)) where $k=\pm B/T$ is the LFM slope. The effect of k is range-doppler coupling at the matched filter output. This effect presents itself as a diagonal ridge in the AF as shown in Figure 4-3.

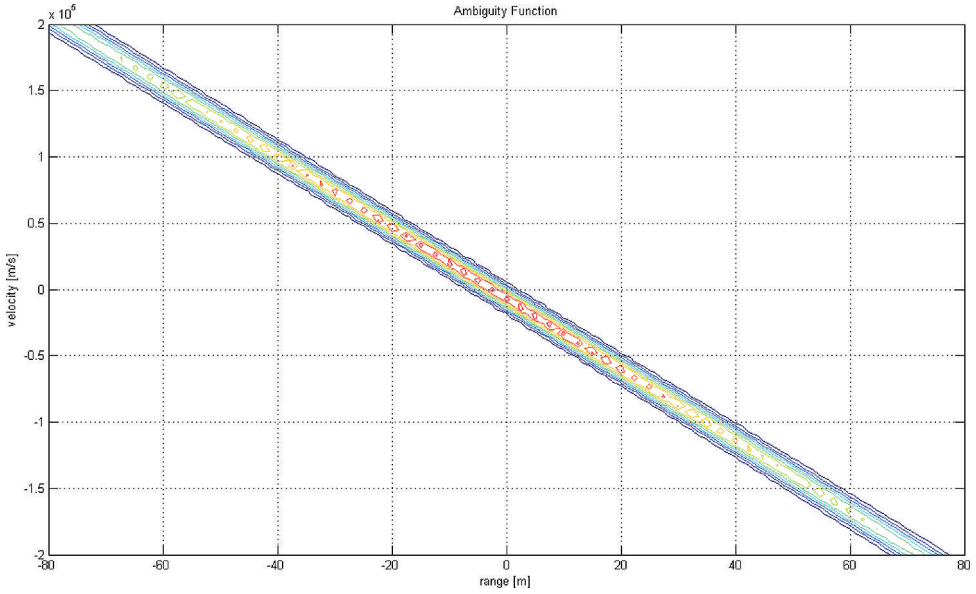

Figure 4-3 AF Contour Plot of a Linear Frequency-modulated Pulse (T=2μs, B=30MHz)

Following Eq. (1.6) using the parameters from section 1.3 a single LFM pulse can either achieve a range resolution of

$$\Delta R_{LFM,LPRF} = \frac{c}{2 \cdot B_{LPRF}} = \frac{3 \cdot 10^8}{2 \cdot 30 \cdot 10^6} \frac{\mathrm{m/s}}{\mathrm{1/s}} = 5\mathrm{m} \tag{4.8}$$

or

$$\Delta R_{LFM,MPRF} = \frac{c}{2 \cdot B_{MPRF}} = \frac{3 \cdot 10^8}{2 \cdot 7.5 \cdot 10^6} \frac{\mathrm{m/s}}{\mathrm{1/s}} = 20\mathrm{m} \tag{4.9}$$

Because the complex envelop of a LFM pulse (as given by Eq. (4.7)) is rectangular it can only achieve the same peak time sidelobe level of -13.2dB as an unmodulated pulse (shown in Figure 2-5). So for a reduction of sidelobe levels filters have to be used. Table 4-1 gives three possible weighting functions and their influence on the peak time sidelobe level. For a more detailed overview on filters we refer again to Harris (1978).

Weighting Function	Peak Time Sidelobe Level
Uniform/Rectangular	-13.2dB
Taylor (-40dB)	-40dB
Hamming	-43dB

Table 4-1 Comparison of LFM Weighting Functions (Skolnik et al. (2008))

4.2.2 Nonlinear Frequency Modulation

Other then LFM, the Nonlinear Frequency Modulation (*NLFM*) does not require frequency domain weighting to reduce time domain sidelobes. This advantage is achieved by decreasing the frequency sweep time in the beginning and the end of the pulse (see Figure 4-4), thus tapering the waveform spectrum so that the matched filter output already provide the desired time sidelobe level. Because no additional filter is needed for sidelobe level reduction NLFM does not suffer from loss in SNR as LFM does (Skolnik et al. (2008)). A comparison of sidelobe levels and SNR of LFM and NLFM is given in Table 4-2.

Signal	Peak Time Sidelobe Level	Matched Filter Loss
LFM, unweighed	-13.2dB	0dB
LFM, Tylor (-40dB)	-40dB	1.15dB
LFM, Hamming	-43dB	1.34dB
NLFM, sine-based	-32.7dB	0dB

Table 4-2 Comparison of LFM and NLFM Waveform Performance (Skolnik et al. (2008))

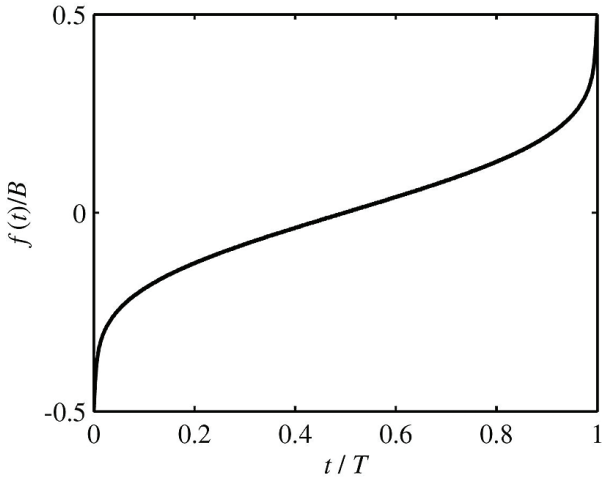

Figure 4-4 Nonsymmetrical Nonlinear Frequency-modulated Pulse (from Levanon and Mozeson (2004))

A NLFM pulse is represented by its complex envelope

$$u(t) = g(t)\exp(j\phi(t)) \tag{4.10}$$

(e.g., Levanon and Mozeson (2004)) where $g(t)$ is the amplitude and $\phi(t)$ the phase function.

As range resolution (Eq. (1.6)) is only influenced by the instantaneous bandwidth (B) available using the parameters from section 1.3 for a single NLFM pulse results in the same range resolution as for a single LFM pulse ($\Delta R_{NLFM,LPRF}=\Delta R_{LFM,LPRF}$ =5m and $\Delta R_{NLFM,MPRF}=\Delta R_{LFM,MPRF}$ =20m, respectively).

NLFM also suffers from range-doppler coupling but other then LFM the ridge degrades and leads to ambiguities with higher Doppler frequencies (Levanon and Mozeson (2004)).

4.2.3 Costas Codes

While LFM and NLFM use continuous functions to sweep a selected frequency band Costas (1984) suggested a discrete frequency coding. In Figure 4-5 a) a LFM pulse and in b) a Costas-coded pulse is shown in a binary matrix representation. Columns represent continuous time slices of duration t_b, and rows represent distinct frequencies (equally spaced by Δf). A dot associates the given time with a frequency transmitted. At any time only one frequency is transmitted and each frequency is only used once (Levanon and Mozeson (2004)).

A Costas-coded pulse is represented by its complex envelope

$$u(t) = \sum_{n=0}^{N-1} u_n(t - n \cdot t_b) \tag{4.11}$$

(e.g., Costas (1984)) where N represents the number of distinct frequencies (in the hopping sequence $a=\{a_1,a_2,\ldots,a_N\}$),

$$u_n(t)=\begin{cases}\exp(j2\pi f_n t), & 0\le t\le t_b\\ 0 & \text{elsewhere}\end{cases} \tag{4.12}$$

and

$$f_n=\frac{a_n}{t_b} \tag{4.13}$$

For an N-element hopping sequence a there is a total number of $N!$ different $N\times N$ binary arrays. Which of these arrays represent a Costas code isn't easily determined. Golomb and Taylor (1984) presented several construction methods for Costas arrays, a subset of which are Welch constructors. The Welch-1 construction method is applicable for any number N with $N=p-1$, where p can be every prime larger than 2. The rows of the array are numbered $i=1,2,\ldots,p-1$, the columns $j=0,1,\ldots,p-2$ and a dot will be put at position $\{i,j\}$ if $i=\alpha^j$, where α is a primitive element in the Galois field[5] GF(p). Every sequence constructed with the Welch-1 method $a_{Welch\text{-}1}$ starts with 1. Removing the first element of $a_{Welch\text{-}1}$ and subtracting 1 from the remaining elements in the sequence creates a Costas sequence of size $N=p-2$. This construction method is called Welch-2.

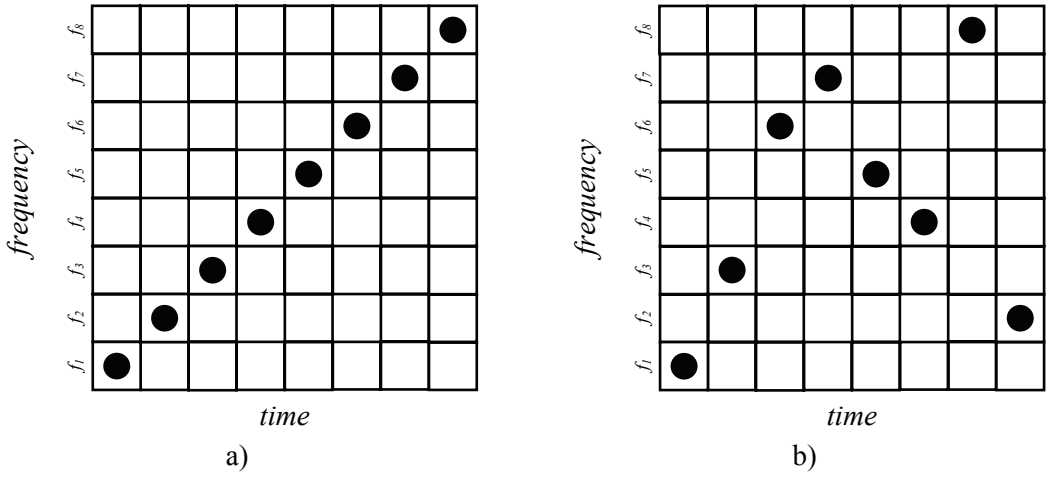

Figure 4-5 Matrix Representation of a) Quantized LFM and b) Costas Coding

The hopping sequence strongly affects the AF of the signal. According to Levanon and Mozeson (2004) the AF of a signal can be roughly predicted by overlaying a copy of the binary matrix repre-

[5] A Galois field or finite field is a field that contains only finitely many elements. There is a unique field of order p^n for every prime p and every possible integer n up to isomorphism (Jacobson (1985)).

sentation on itself, and then shifting one relative to the other according to the desired delay (horizontally) and Doppler (vertically). The peak of the AF that can be expected for a given delay-Doppler shift depends on the number of coinciding grid points[6] (M) and is approximately M/N at the corresponding delay-Doppler coordinate. What is unique for a Costas-coded signal is that the number of coinciding grid points cannot be larger than one for all but the zero-shift case. An example for this construction method is shown in Figure 4-6 using an 8-element Costas-coded pulse. Figure 4-7 confirms the thumbtack-like shape of the AF predicted for this pulse.

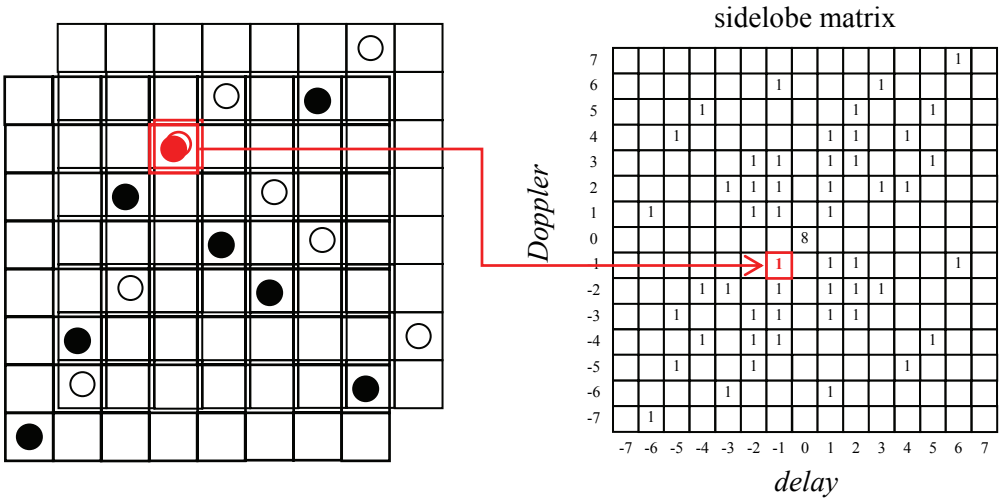

Figure 4-6 AF Sidelobe Prediction from Binary Matrix Representation

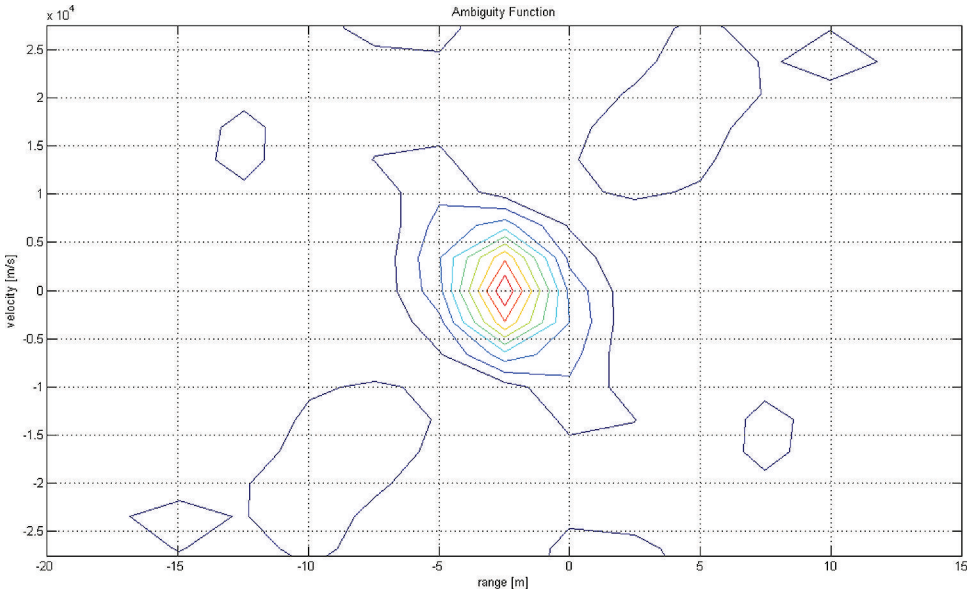

Figure 4-7 AF Contour Plot of an 8-element Costas-coded Pulse (T=2μs)

[6] Grid points refer to delay and Doppler shifts which are integer multiples of t_b and Δf, respectively.

4.3 Phase-coded Pulses

Like Costas codes, phase-coded waveforms subdivide a pulse into a number of subpulses (or bits) of duration

$$t_b = \frac{\tau_P}{N} \tag{4.14}$$

(e.g., Ludloff (2002)). They can be separated based on the phase modulation applied to each subpulse (Skolnik et al. (2008)).

4.3.1 Binary Barker Codes

In a binary phase (or biphase) code the phase of a single subpulse is selected to be either *0* or π radians. If the selection of the phase is made at random, the waveform approximates a noise-modulated signal, thus having a thumbtack-like AF. On the other hand completely random selection of phases leads to higher sidelobe levels than required (Skolnik (2001)).

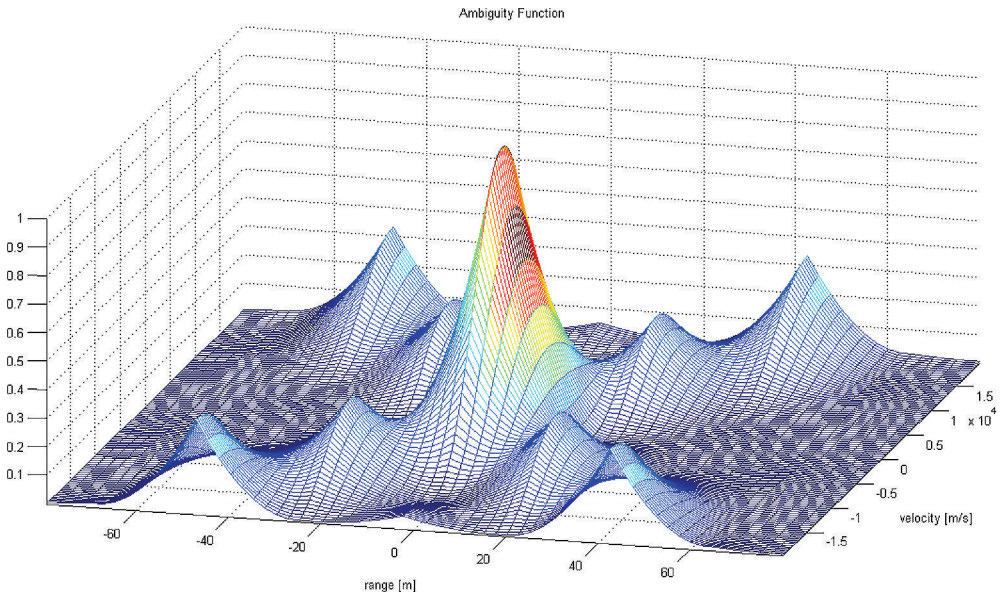

Figure 4-8 AF of a 13-bit Barker-coded Pulse (T=2µs)

Depending on the sequence of random phase selection higher or lower maximum sidelobe levels can be achieved. A special group of phase codes are Barker codes where the subpulse phases are arranged as to distribute the energy in the sidelobe region uniformly, thus resulting in equal range delay sidelobe levels. Figure 4-9 shows the phase alternations between *0* an π radians in accordance

with the code sequence. A list of all known binary Barker codes including their peak time sidelobe levels is given in Table 4-3.

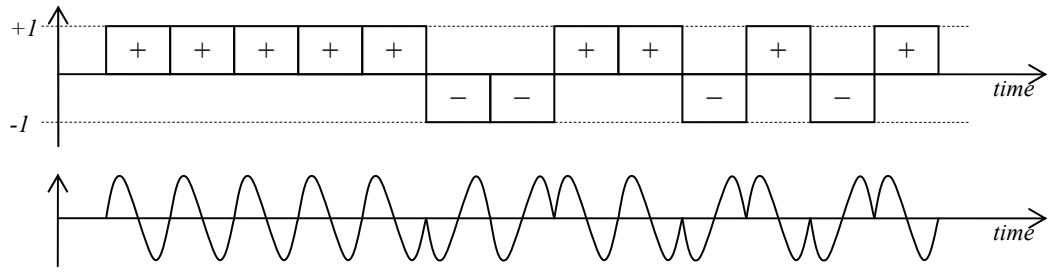

Figure 4-9 13-bit Barker-coded Signal

Code Length	Code Sequence	Peak Time Sidelobe Level
2	++ ; +−	-6.0dB
3	++−	-9.5dB
4	++−+ ; +++−	-12.0dB
5	+++−+	-14.0dB
7	+++−−+−	-16.9dB
11	+++−−−+−−+−	-20.8dB
13	+++++−−++−+−+	-22.3dB

Table 4-3 Known Binary Barker Codes (Skolnik (2001))

A Barker-coded pulse is represented by its complex envelope

$$u(t) = \frac{1}{\sqrt{T}} \sum_{n=0}^{N-1} u_n \operatorname{rect}\left(\frac{t - n \cdot t_b}{t_b} \right) \tag{4.15}$$

(e.g., Levanon and Mozeson (2004)) where N represents the length of the phase code sequence $\phi=\{\phi_1,\phi_2,\ldots,\phi_N\}$ and

$$u_n = \exp(j\phi_n) \tag{4.16}$$

4.3.2 Nested Barker Codes

Till today, there exists no Barker code other then those given in Table 4-3. This means that Barker coded signals are limited to time-bandwidth products of BT=13 which is a relatively low value. To overcome this problem an early method was to generate codes of length N>13 by nesting codes of shorter length. Levanon and Mozeson (2004) demonstrate this concept by using Barker codes of length *3* (u_n={+ + −}) and *13* (v_n={+ + + + + − − + + − + − +}) to form an 39-element code. When

u is used as outer code and v as inner ($v \otimes u$) then the nested 39-element Barker code would result as shown in Figure 4-10.

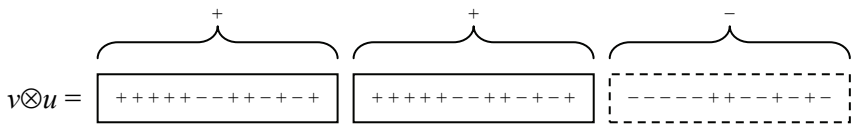

Figure 4-10 Nested 39-element Barker Code

The Autocorrelation Function (*ACF*) for $v \otimes u$ is shown in Figure 4-11.

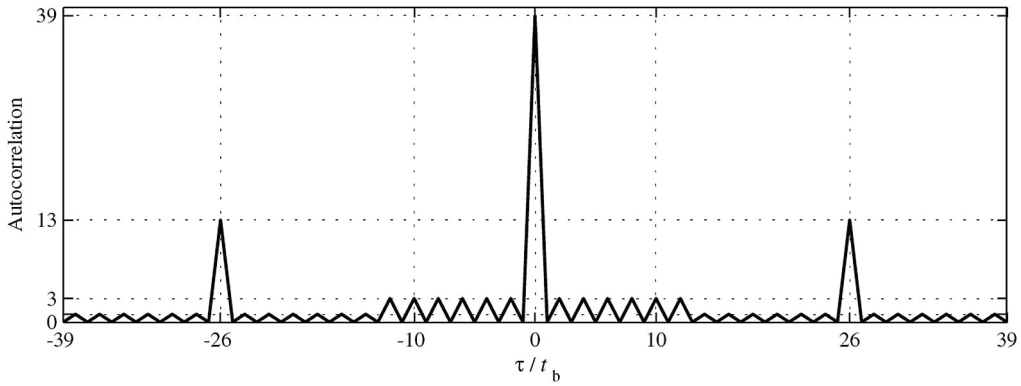

Figure 4-11 ACF of a Nested 39-element Barker Code (from Levanon and Mozeson (2004))

4.3.3 P4 Polyphased Code

One of the drawbacks of Binary Barker Codes (see subsection 4.3.1) and Nested Barker Codes (see subsection 4.3.2) is their low Doppler tolerance. They were optimized for time delay sidelobe reduction (Levanon and Mozeson (2004)). As can be seen from Figure 4-8, the delay sidelobe levels of, i.e., a 13-element Barker-coded pulse are much higher than those predicted from observing only the zero-Doppler cut, once the returned signal is Doppler shifted. Other than Barker codes with their random phase code sequence polyphase codes are based on the phase history of FM pulses. That is why they are also referred to as chirplike phase codes (Levanon and Mozeson (2004)).

The P4 Polyphased Code introduced by Lewis and Kretschmer (1982) is based on the phase history of LFM pulses and has good aperiodic properties. It is given by its complex envelope (Eq. (4.15) and Eq. (4.16)), with

$$\phi_n = \frac{2\pi}{N}(n-1)\left(\frac{n-1-N}{2}\right) \tag{4.17}$$

(e.g., Levanon and Mozeson (2004)) where $1 \le n \le N$ for any $N \in \mathbf{N}$.

As P4 codes are based on LFM pulses their AFs have similar regularities. From comparison of an AF plot of a 16-bit P4-coded pulse (Figure 4-12) with that of a LFM pulse (Figure 4-3) it can be seen that P4 codes inherit the range-doppler coupling, expressing itself in the diagonal ridge. Characteristic for P4 codes is the amplitude of the ridge, first falling and than rising again with higher Doppler. This results from using only one sample of a LFM pulse for each bit of the P4 code. The more samples would be used, the more the ridge would approach that of a LFM pulse. (Ludloff (2002)).

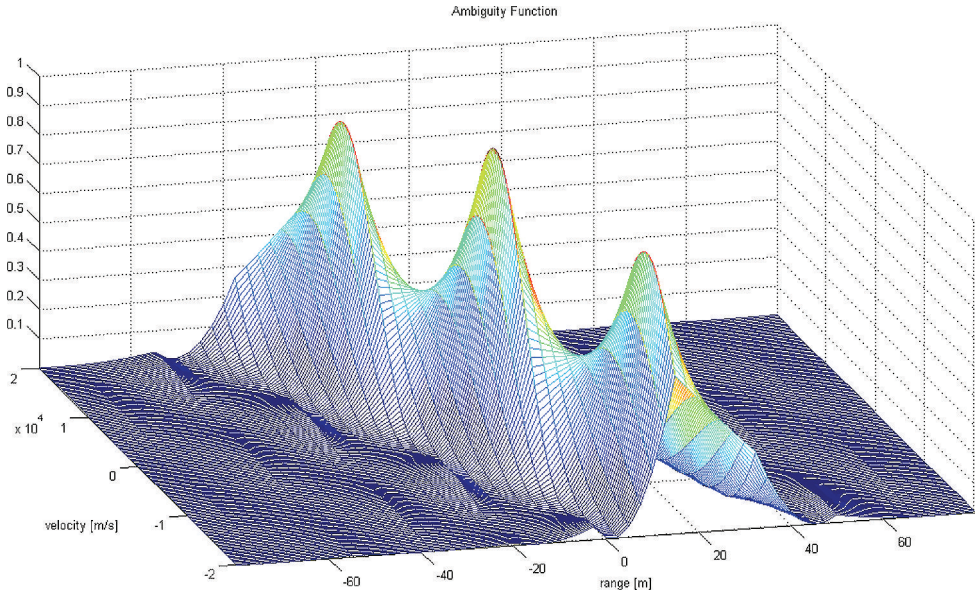

Figure 4-12 AF of a 16-bit P4-coded Pulse (T=2µs)

One advantage of a P4 code is the low sidelobe level that can be achieved. It can be reduced to ~-26dB (see Table 4-4) before it starts to rise again for code lengths of N>100. Ludloff (2002) showed that a reduction of more then -40dB is possible, i.e., for a 13-bit P4 code, if the concept of mismatched filtering is used instead of a matched filter.

Code Length	Peak Time Sidelobe Level
10	-16dB
40	-22dB
100	-26dB

Table 4-4 Sidelobe Levels for Different Code Lengths of P4-coded Pulses (Ludloff (2002))

A second advantage is the Doppler-tolerance (shown by Kretschmer and Lewis (1983)) which allows for simplified receiver hardware with only negligible degradation in performance (Levanon and Mozeson (2004)).

4.4 Frequency-modulated Pulse Train

For a single pulse the Doppler resolution is $1/\tau_P$. So a good Doppler resolution requires a long signal. On the other hand, in monostatic radar systems (transmitter and receiver use the same antenna) the receiver is blocked while a pulse is transmitted, thus making the radar system "miss" all incoming signals during that time (eclipsing). So to minimize eclipsing a short signal is required.

One solution to meet both requirements is to use a coherent[7] train of pulses. In many practical cases these pulses are modulated for the same reasons as single pulses are – to achieve wider bandwidth, hence better range resolution, or sidelobe reduction. In addition to intrapulse modulation (e.g., LFM) a train of pulses offers the possibility to introduce diversity between the pulses (interpulse modulation) to obtain additional advantages, such as lower delay sidelobes or lower recurrent lobes (Levanon and Mozeson (2004)).

A train of LFM pulses (see Figure 4-13) is probably the most popular radar signal in airborne radar (Stimson (1998)), where each pulse is transmitted on the same carrier frequency.

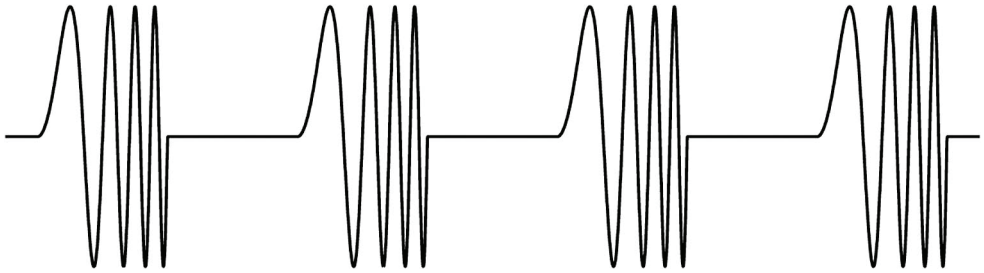

Figure 4-13 Coherent Train of Uniform Linear Frequency-modulated Pulses (from Levanon and Mozeson (2004))

A coherent linear frequency-modulated train of N pulses is represented by its complex envelope

$$u(t) = \frac{1}{\sqrt{N}} \sum_{n=0}^{N-1} u_n(t - n \cdot T_P) \tag{4.18}$$

(e.g., Levanon and Mozeson (2004)) where $u_n(t)$ is the complex envelope of a single LFM pulse as given by Eq. (4.7). Uniformity of the pulses is expressed by $u_n(t)=u_1(t)$.

The main advantage of this type of signal is the improved Doppler resolution by the factor N. Due to the use of identical LFM pulses the time sidelobe properties of the main peak are identical to those of a single LFM pulse (Levanon and Mozeson (2004)). From section 1.3 it follows that for this signal $\Delta R_{CTLFM,LPRF}=\Delta R_{LFM,LPRF}$ =5m and $\Delta R_{CTLFM,MPRF}=\Delta R_{LFM,MPRF}$ =20m, respectively.

[7] In this case coherency means that the receiver “knows” the original initial phase of each pulse of the signal.

4.5 Stepped-frequency Waveform

All signals for achieving high range resolution introduced so far suffer from the following limitation: The instantaneous bandwidth available for a single pulse (see section 1.3) is too low as to achieve the range resolution required for classification capability (see subsection 3.5.1).

Ruttenberg and Chanzit (1968) were the first to describe a method to obtain high range resolution by using a frequency-stepped pulse train, without requiring a coherent transmitter for frequency generation. This concept was picked up by Einstein (1984), who investigated Stepped-Frequency (*SF*) pulse trains for use in HRR, thus starting a broad research effort on stepped-frequency waveforms. Up to today, research topics included, i.e., the generation of stepped-frequency waveforms (e.g., Paulose (1994)) as well as their tailoring for special radar needs (e.g., Prodi and Tilli (2007) (motion compensation) or Feixing et al. (2006) (resolving ambiguities)) or their practical application for target recognition (e.g., van der Heiden and de Vries (1996)).

A stepped-frequency waveform achieves its high range resolution by transmitting the required signal bandwidth not within a single pulse but as a sequence of *N* pulses, where each pulse is transmitted on a different carrier frequency (see Figure 4-14). It is an interpulse modulation and can be applied to trains of unmodulated as well as modulated (e.g., LFM) pulses.

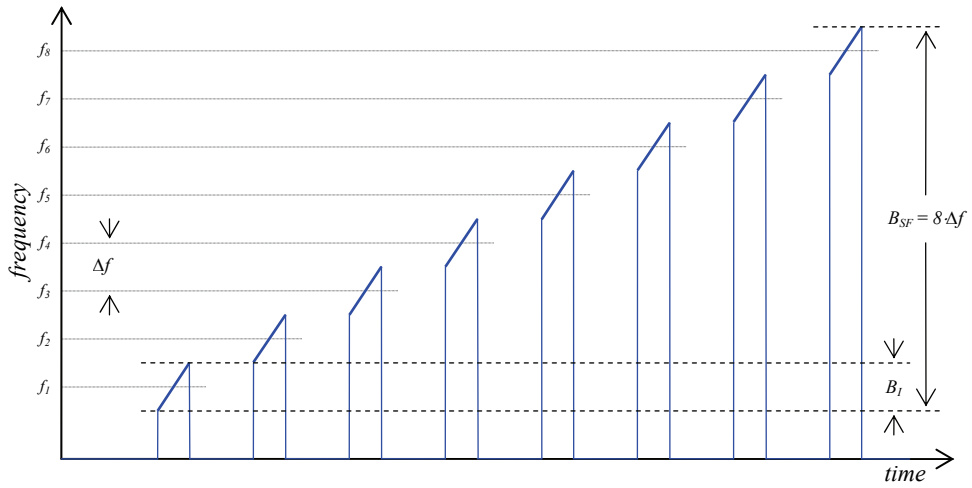

Figure 4-14 Linear Stepped-frequency Waveform of 8 LFM Pulses

Using *N* uniformly spaced frequency steps of size Δf Einstein (1984) showed that the range resolution (ΔR) of a RRP resulting from a stepped-frequency waveform is equal to the reciprocal of the stepped-frequency pulse train bandwidth (B_{SF}):

$$\Delta R_{SF} = \frac{c}{2 \cdot N \cdot \Delta f} = \frac{c}{2 \cdot B_{SF}} \tag{4.19}$$

In the following subsections we will use the parameters from section 1.3 to analyse the concept of SF pulse trains. While in both burst modes the carrier frequency can be changed from burst to burst, the LPRF burst also allows for a carrier frequency change between pulses. The second advantage of the LPRF burst is the higher instantaneous bandwidth available. From this it follows, that for delivering the bandwidth necessary (B=200MHz, see subsection 3.5.1) for achieving good classification results it would take at least 18s using MPRF bursts (4 bursts on object per scan interval (2s) under optimal conditions, $B_{Pulse}=B_{Burst}$=7.5MHz, Δf_{min}=5MHz) while only one LPRF burst (3ms) would suffice (B_{Pulse}=30MHz, Δf=25MHz, N=8, B_{Burst}=205MHz). For that reason the analyses are limited to the LPRF burst (τ_P=2µs, T_P=375µs, N=8) only.

4.5.1 Interpulse Modulation (Linearly Stepped) & Intrapulse Modulation (LFM)

Here we analyse the LPRF burst with LFM (B=30MHz) as intrapulse modulation and linear SF (Δf=const.=15MHz) as interpulse modulation.

From that we would expect a range resolution of

$$\Delta R_{LSF15,LFM} = \frac{c}{2 \cdot B_{LSF15}} = \frac{3 \cdot 10^8}{2 \cdot (15 + 7 \cdot 15 + 15) \cdot 10^6} \frac{\mathrm{m/s}}{1/\mathrm{s}} = 1.111\mathrm{m} \tag{4.20}$$

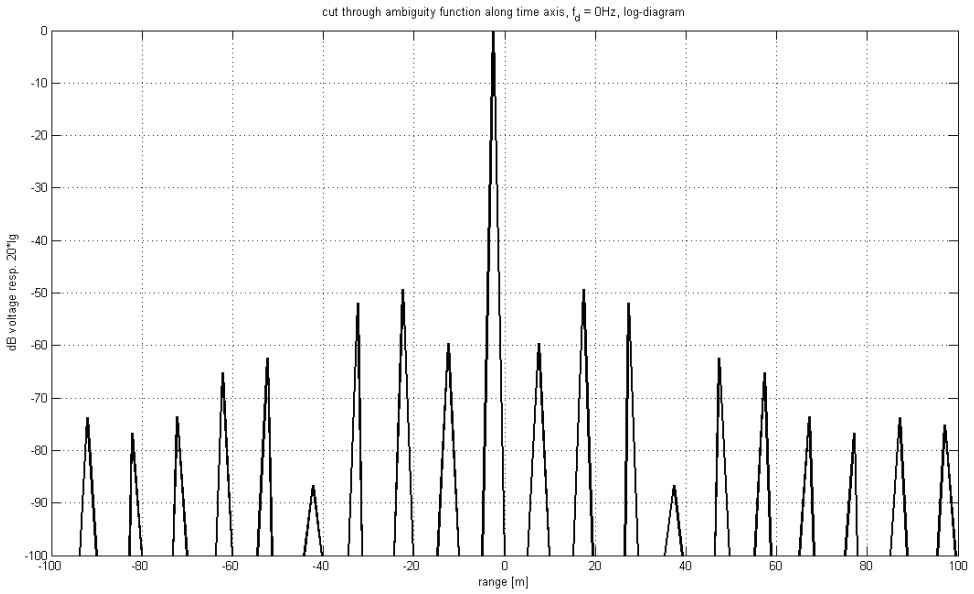

Figure 4-15 Main Peak Cut of an 8-LFM-element Linear Frequency-stepped Waveform (τ_P=2µs, T_P=375µs, B=30MHz, Δf=15MHz)

Other than expected from Eq. (4.20), the result of the toolbox analysis suggests that with this burst form a range resolution of $\Delta R_{LSF15,LFM} \cong$0.3m can be achieved. And even though the sidelobe

levels of the main peak (Figure 4-15) are much lower then would be expected from a single LFM pulse (see subsection 4.2.1), -49dB compared to -13.2dB, the overall side peak level (Figure 4-16) of the signal rises up to -19dB.

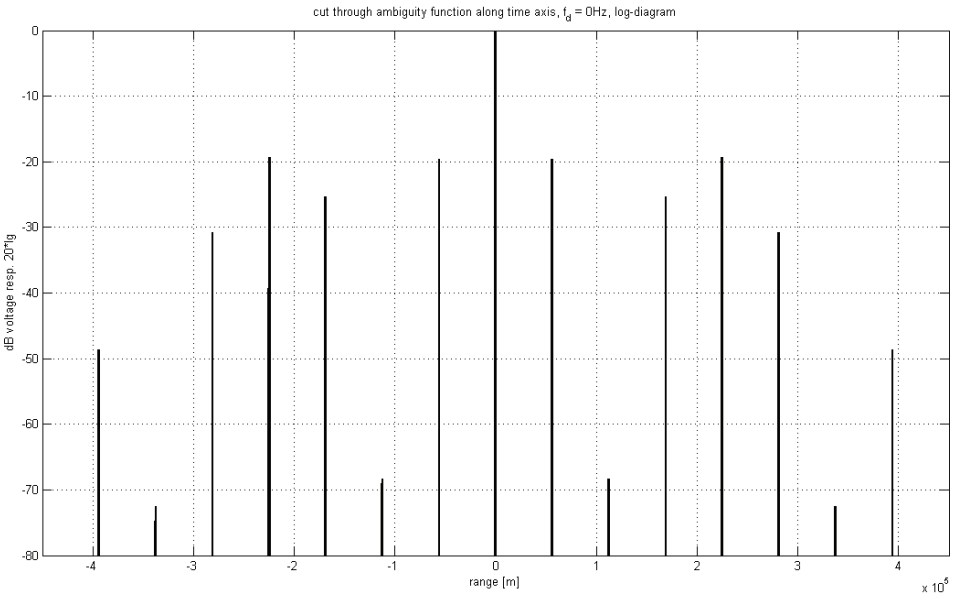

Figure 4-16 Side Peaks Cut of an 8-LFM-element Linear Frequency-stepped Waveform (τ_P=2µs, T_P=375µs, B=30MHz, Δf=15MHz)

Next we analyse the LPRF burst still with LFM (B=30MHz) as intrapulse modulation but with linear SF (Δf=const.=25MHz) as interpulse modulation.

Similar to Eq. (4.20), we calculate the range resolution for this signal to be

$$\Delta R_{LSF25,LFM} = \frac{c}{2 \cdot B_{LSF25}} = \frac{3 \cdot 10^8}{2 \cdot (15 + 7 \cdot 25 + 15) \cdot 10^6} \frac{\mathrm{m/s}}{\mathrm{1/s}} = 0.732\mathrm{m} \tag{4.21}$$

but going from the analysis results for Δf=15MHz, we would expect a further improved range resolution as to $\Delta R_{LSF25,LFM} \leq \Delta R_{LSF15,LFM} \cong 0.3\mathrm{m}$.

The toolbox results suggest that with this burst a range resolution of only $\Delta R_{LSF25,LFM} \cong 0.65\mathrm{m}$ is possible which is still better then calculated in Eq. (4.21) but not as good as expected. And while the sidelobe level of the main peak (Figure 4-17) is nearly identical to that for Δf=15MHz, -48dB compared to -49dB, the overall side peak level (-12.5dB) also performs poorer.

This could be explained by property (2) of the AF (Eq. (4.4)) and would imply that the volume distribution of the AF along the Doppler delay axis for Δf=25MHz is concentrated closer to the origin thus leading to reduced sidelobe levels for higher Doppler frequencies (Levanon and Mozeson (2004)).

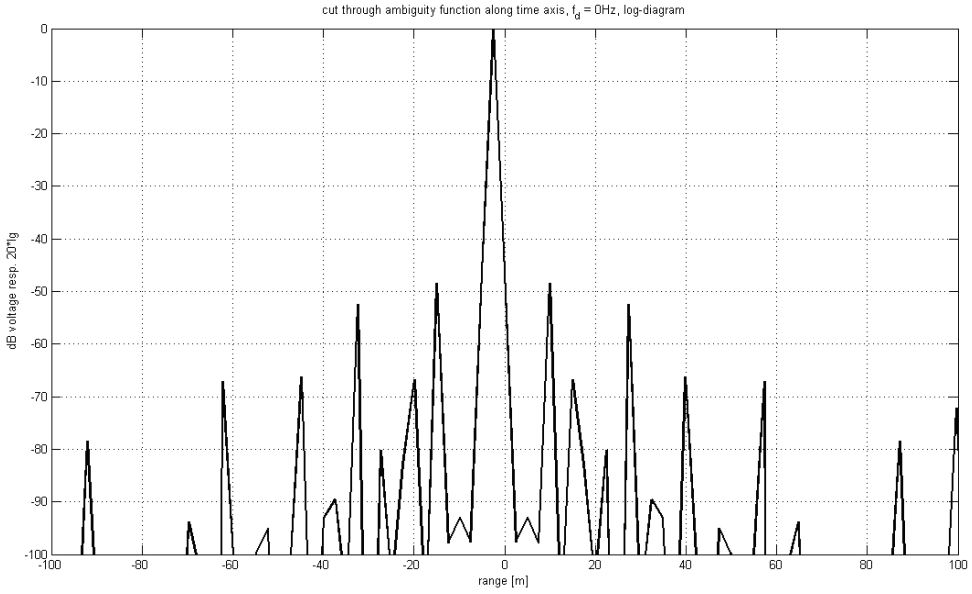

Figure 4-17 Main peak Cut of an 8-LFM-element Linear Frequency-stepped Waveform (τ_P=2µs, T_P=375µs, B=30MHz, Δf=25MHz)

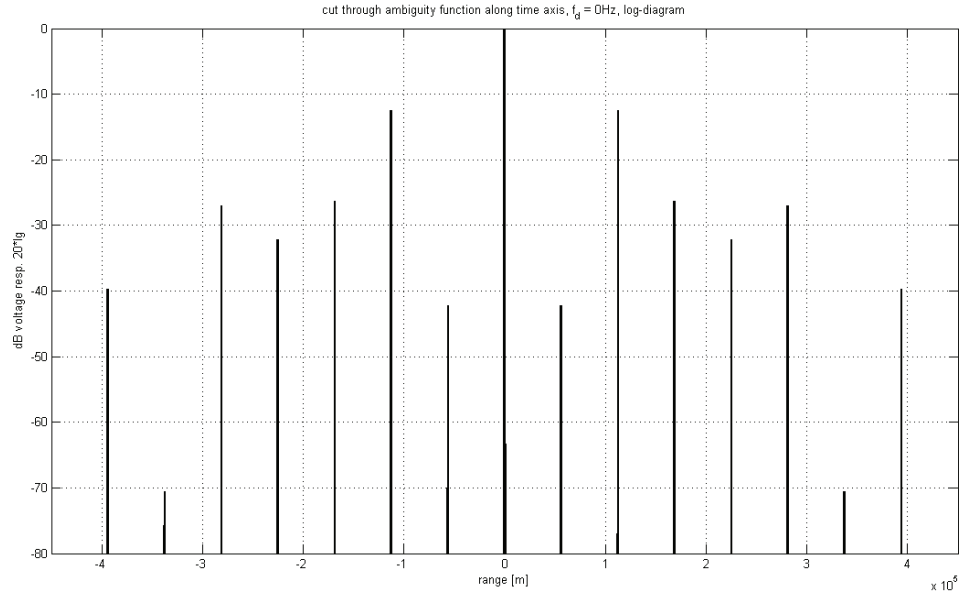

Figure 4-18 Side Peaks Cut of an 8-LFM-element Linear Frequency-stepped Waveform (τ_P=2µs, T_P=375µs, B=30MHz, Δf=25MHz)

Now the interpulse modulation will be linear SF with Δf=const.=30MHz and we calculate the range resolution to

$$\Delta R_{LSF30,LFM} = \frac{c}{2 \cdot B_{LSF30}} = \frac{3 \cdot 10^8}{2 \cdot (8 \cdot 30) \cdot 10^6} \frac{\text{m/s}}{\text{1/s}} = 0.625\text{m} \tag{4.22}$$

The result of the toolbox analysis suggests that with this burst form the same range resolution of $\Delta R_{LSF30,LFM} \cong 0.3$m as for Δf=15MHz can be achieved. A closer look at the main peak (Figure 4-19) shows that also the same side lobe level (-49dB) is reached, while the overall side peak level (Figure 4-20) rises up to -12dB, but showing a more equally distributed volume then for Δf=15MHz or Δf=25MHz.

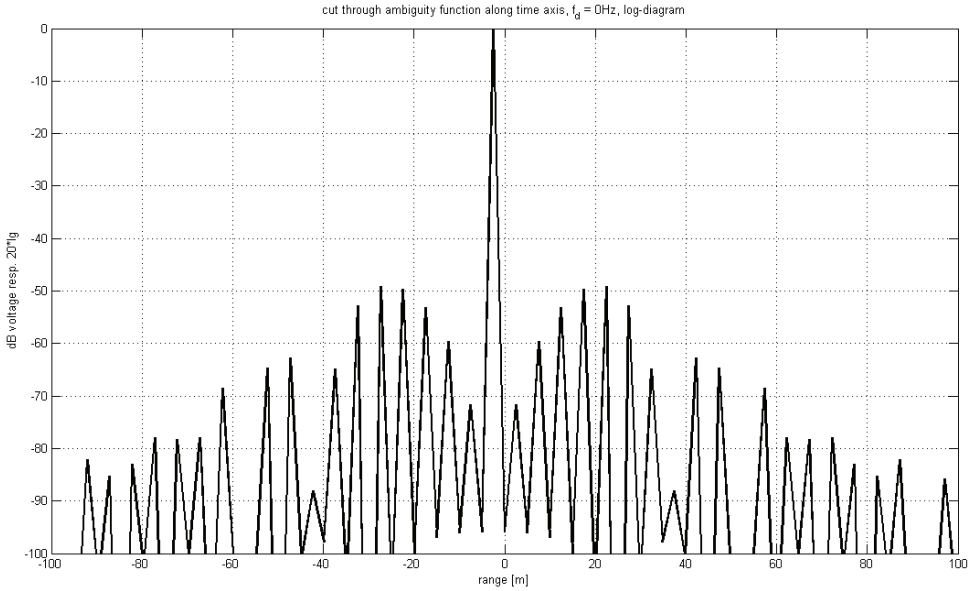

Figure 4-19 Main Peak Cut of an 8-LFM-element Linear Frequency-stepped Waveform (τ_P=2µs, T_P=375µs, B=30MHz, Δf=30MHz)

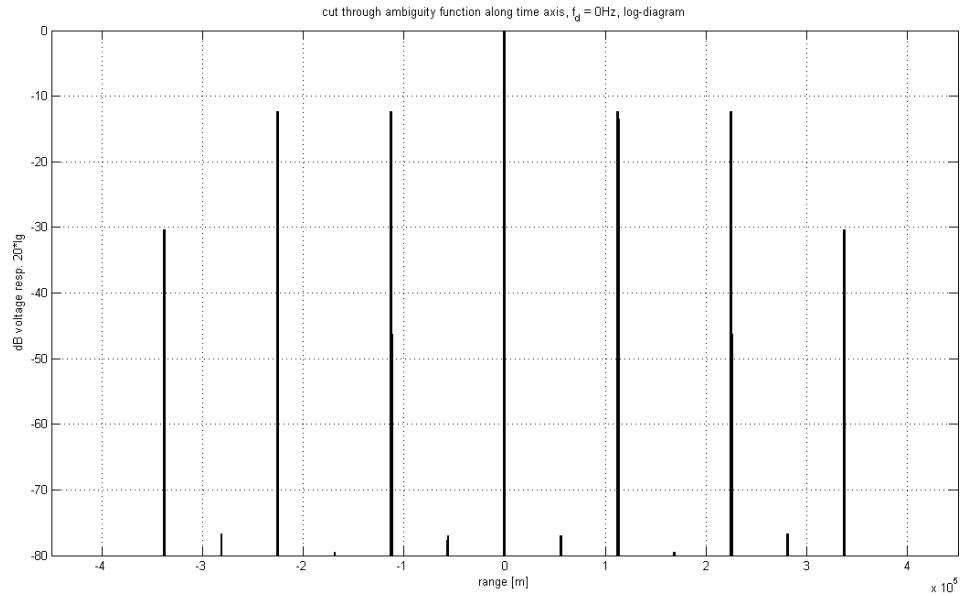

Figure 4-20 Side Peaks Cut of an 8-LFM-element Linear Frequency-stepped Waveform (τ_P=2µs, T_P=375µs, B=30MHz, Δf=30MHz)

From the 3 analysed signals a frequency step of Δf=25MHz seems to be a good compromise between an equal, overall volume distribution along time delay and grating lobes for higher Doppler frequencies. Also frequency steps of 15MHz would

4.5.2 Interpulse Modulation (Linearly Stepped) & Intrapulse Modulation (NLFM)

Here we analyse the LPRF burst with NLFM (B=30MHz) as intrapulse modulation and linear SF (Δf=const.=25MHz) as interpulse modulation.

Equal to Eq. (4.21), as the same Δf and B are used, we would expect the range resolution of this burst to be $\Delta R_{LSF25,NLFM}=\Delta R_{LSF25,LFM}$=0.732m. But the analysis shows that only a range resolution of $\Delta R_{LSF25,NLFM}\cong$49m can be achieved, which is much worse then that of a single NLFM pulse (see subsection 4.2.2).

An explanation for this result could be that the special properties of the NLFM, faster frequency sweep in the beginning and at the end of the instantaneous bandwidth interval, is the same frequency region where the single pulses overlap in the frequency domain, resulting in phase effects that would need additional research.

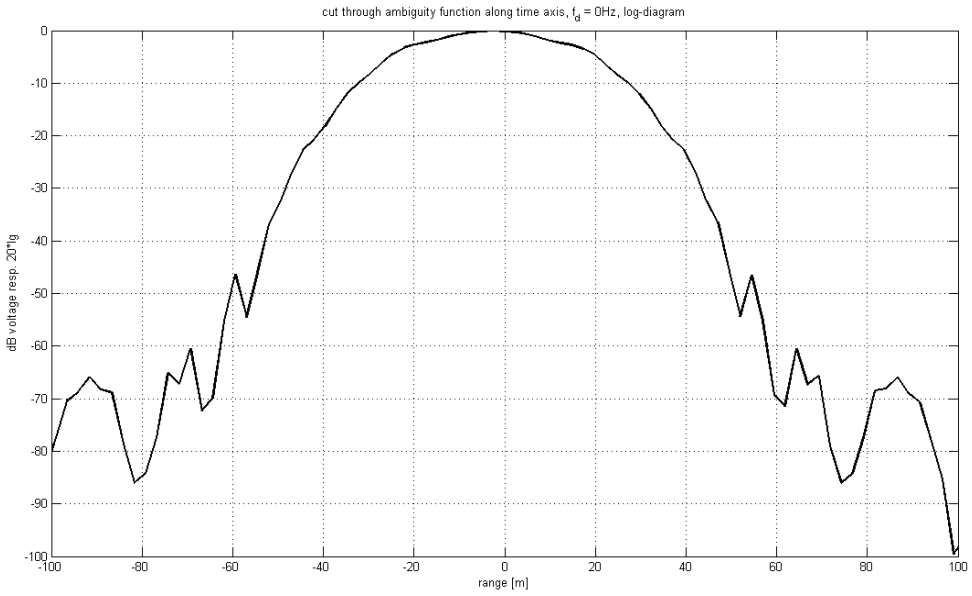

Figure 4-21 Main Peak Cut of an 8-NLFM-element Linear Frequency-stepped Waveform (τ_P=2µs, T_P=375µs, B=30MHz, Δf=25MHz)

The sidelobe level performance of this signal is as poor as its range resolution. For the main peak (Figure 4-21) the 1st sidelobe rises to -46dB but has no significant gap to its neighbouring values. And the overall side peak level (Figure 4-22) rises up to -11dB.

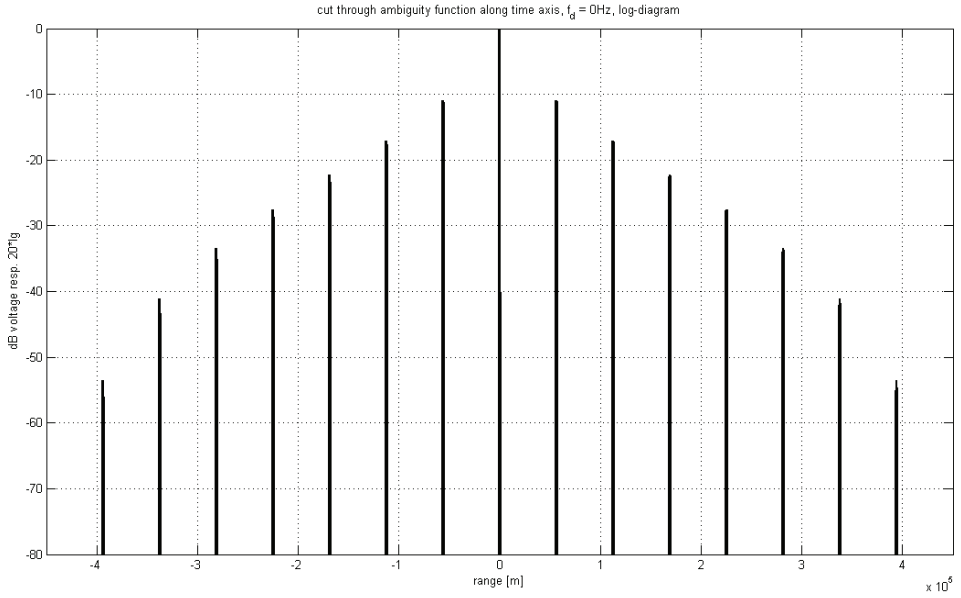

Figure 4-22 Side Peaks Cut of an 8-NLFM-element Linear Frequency-stepped Waveform (τ_P=2µs, T_P=375µs, B=30MHz, Δf=25MHz)

4.5.3 Interpulse Modulation (Linearly Stepped) & Intrapulse Modulation (Barker)

Here we analyse the LPRF burst with a Barker code (M=13) as intrapulse modulation and linear SF (Δf=const.=25MHz) as interpulse modulation.

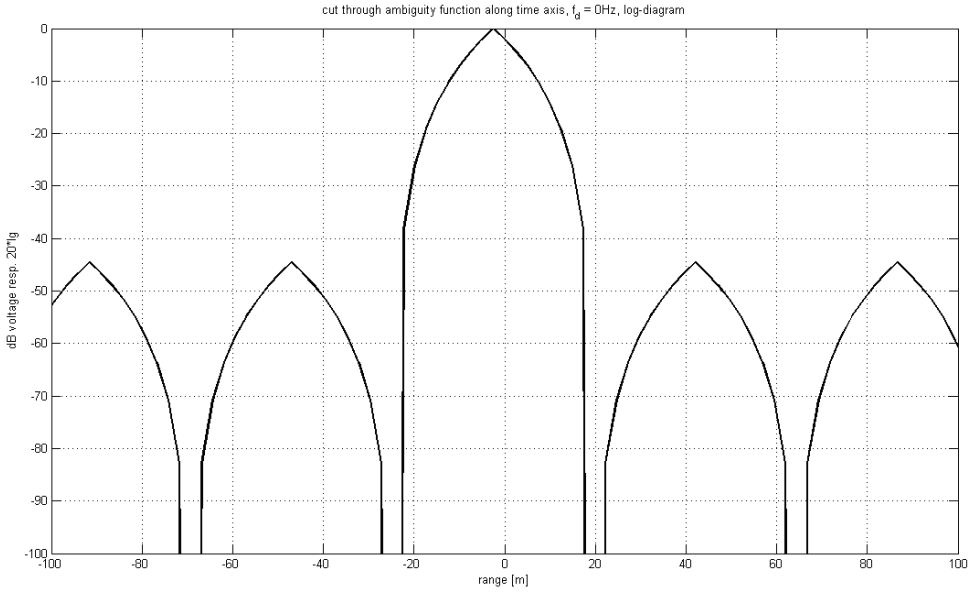

Figure 4-23 Main Peak Cut of an 8-element, 13-bit Barker-coded, Linear Stepped-frequency Waveform (τ_P=2µs, T_P=375µs, Δf=25MHz)

For a phase-coded SF waveform the effective bandwidth B_{SF} can be expressed as

$$B_{PCSF} = (N-1)\Delta f + \frac{1}{t_b} \tag{4.23}$$

(e.g., Temple et al. (2004)) resulting in an achievable range resolution of

$$\Delta R_{PCSF} = \frac{c}{2 \cdot \left((N-1)\Delta f + \frac{M}{\tau_P} \right)} \tag{4.24}$$

Following Eq. (4.24) the 13-bit Barker-coded LPRF burst can be expected to achieve a range resolution of

$$\Delta R_{LSF25,BARK13} = \frac{3 \cdot 10^8}{2 \cdot \left((8-1) \cdot 25 \cdot 10^6 + \frac{13}{2 \cdot 10^{-6}} \right)} \frac{\mathrm{m/s}}{\mathrm{1/s}} = 0.826\mathrm{m} \tag{4.25}$$

The analysis shows that a range resolution of only $\Delta R_{LSF25,BARK13} \cong 13\mathrm{m}$ can be achieved. And while the sidelobe level of the main peak (Figure 4-23) achieves a level of -44dB, the overall side peak level performance of this signal with -2dB is the worst of all signals analysed in this thesis.

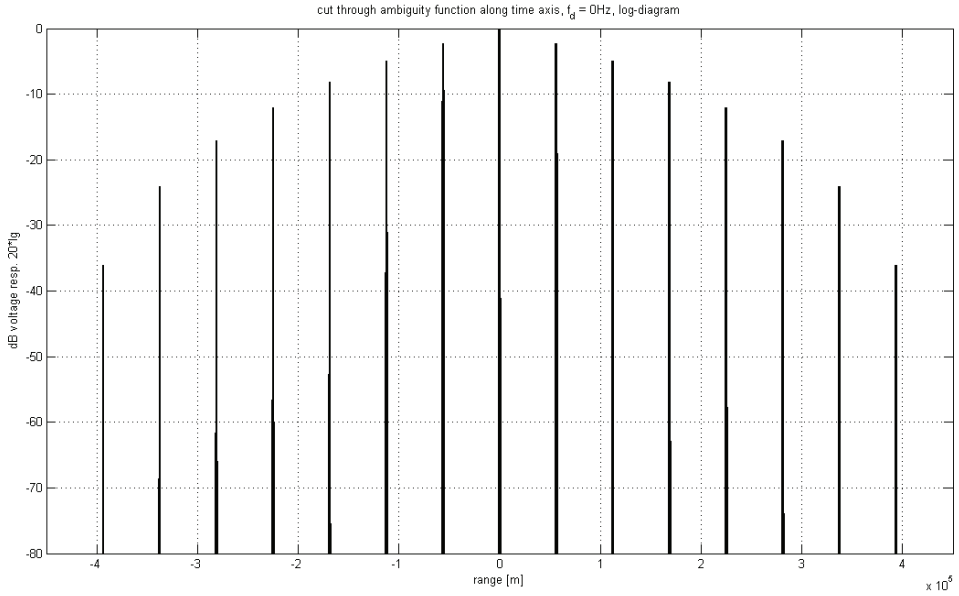

Figure 4-24 Side Peaks Cut of an 8-element, 13-bit Barker-coded, Linear Stepped-frequency Waveform (τ_P=2µs, T_P=375µs, Δf=25MHz)

4.5.4 Interpulse Modulation (Linearly Stepped) & Intrapulse Modulation (P4)

Here we analyse the LPRF burst with a P4 code (M=120, matched filtering) as intrapulse modulation and linear SF (Δf=const.=25MHz) as interpulse modulation.

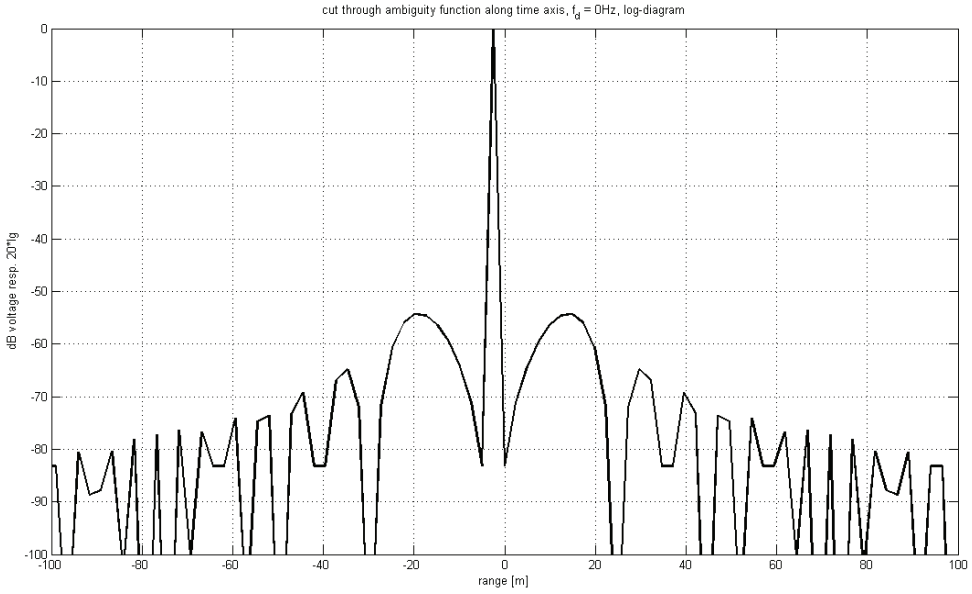

Figure 4-25 Main Peak Cut of an 8-element, 120-bit P4-coded, Linear Stepped-frequency Waveform (τ_P=2µs, T_P=375µs, Δf=25MHz)

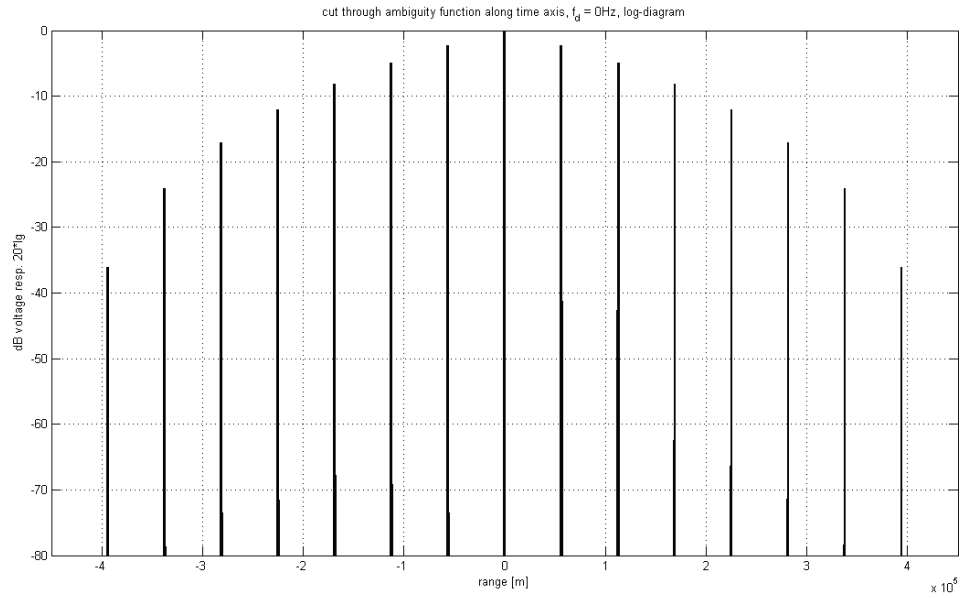

Figure 4-26 Side Peak Cut of an 8-element, 120-bit P4-coded, Linear Stepped-frequency Waveform (τ_P=2µs, T_P=375µs, Δf=25MHz)

For τ_P=2µs and T_S=16.6ns the chosen code length of M=120 is the maximal length possible for which Eq. (4.24) suggests that a range resolution of

$$\Delta R_{LSF25,P4-120} = \frac{3\cdot 10^8}{2\cdot\left((8-1)\cdot 25\cdot 10^6 + \dfrac{120}{2\cdot 10^{-6}}\right)}\frac{\mathrm{m/s}}{\mathrm{1/s}} = 0.638\mathrm{m} \tag{4.26}$$

can be achieved.

The analysis of this burst shows that a range resolution of $\Delta R_{LSF25,P4} \cong 0.35$m can be expected with a main peak sidelobe level (Figure 4-25) of -54dB, the best value of all analysed signals, and an overall side peak level (Figure 4-26) of -2dB, which is as worse as that of a SF waveform with Barker-coded pulses (see subsection 4.5.3).

4.5.5 Interpulse Modulation (Costas Stepped) & Intrapulse Modulation (LFM)

Now we analyse the LPRF burst with LFM (B=30MHz) as intrapulse modulation but with a Costas-ordered SF (Δf=const.=25MHz) as interpulse modulation. The frequency hopping order is based on the 8-element Costas array $a=\{1,3,6,7,5,4,8,2\}$.

When we compare the results of the analysis of this burst with the results from subsection 4.5.2 where the same intrapulse modulation is used, two points need to be mentioned:

1) The comparison of the main peaks of linear (Figure 4-17) and Costas-ordered stepped-frequency (Figure 4-27) shows that the interpulse modulation does not influence the main peak and the range resolution of the signal.

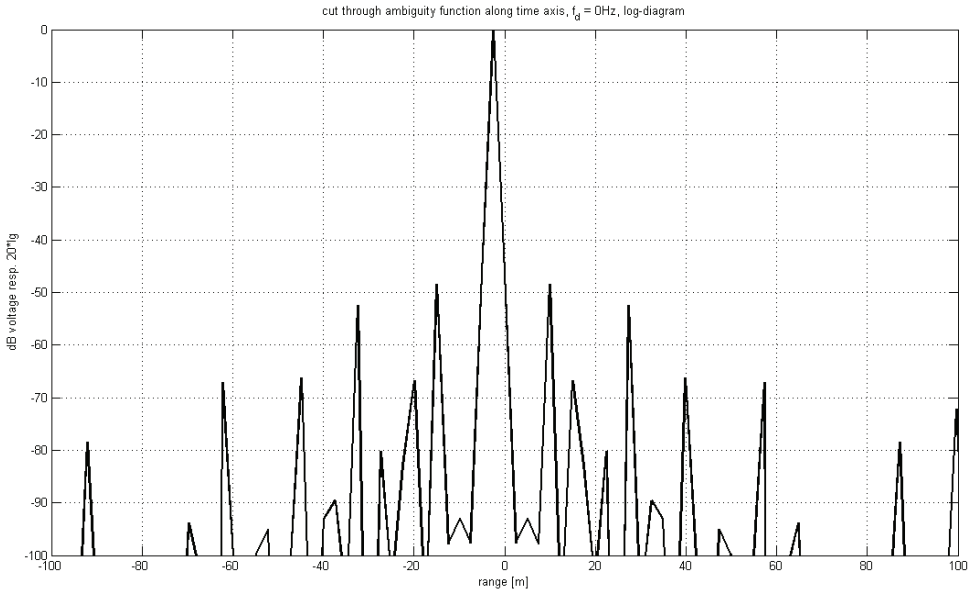

Figure 4-27 Main peak Cut of an 8-LFM-element, Costas-ordered Frequency-stepped Waveform (τ_P=2µs, T_P=375µs, B=30MHz, Δf=25MHz)

2) The comparison of the side peaks of linear (Figure 4-18) and Costas-ordered stepped-frequency (Figure 4-28) shows that the interpulse modulation can reduce the overall side peak level remarkably. In this case from -12.5dB to -39dB.

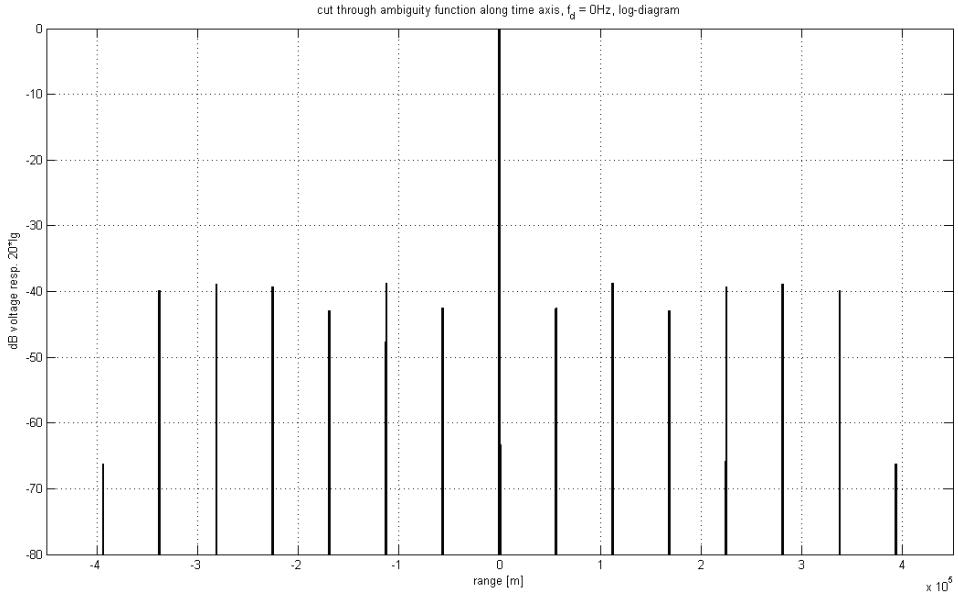

Figure 4-28 Side peak Cut of an 8-LFM-element, Costas-ordered Frequency-stepped Waveform (τ_P=2µs, T_P=375µs, B=30MHz, Δf=25MHz)

4.5.6 Interpulse Modulation (Barker Code) & Intrapulse Modulation (LFM)

The same result of overall side peak level reduction as with Costas-ordered frequency steps can also be achieved by using linear frequency steps but coding the single pulses following binary Barker codes. This is shown in Figure 4-29, where a nested 4⊗2 Barker code has been used resulting in an overall side peak level of -30dB.

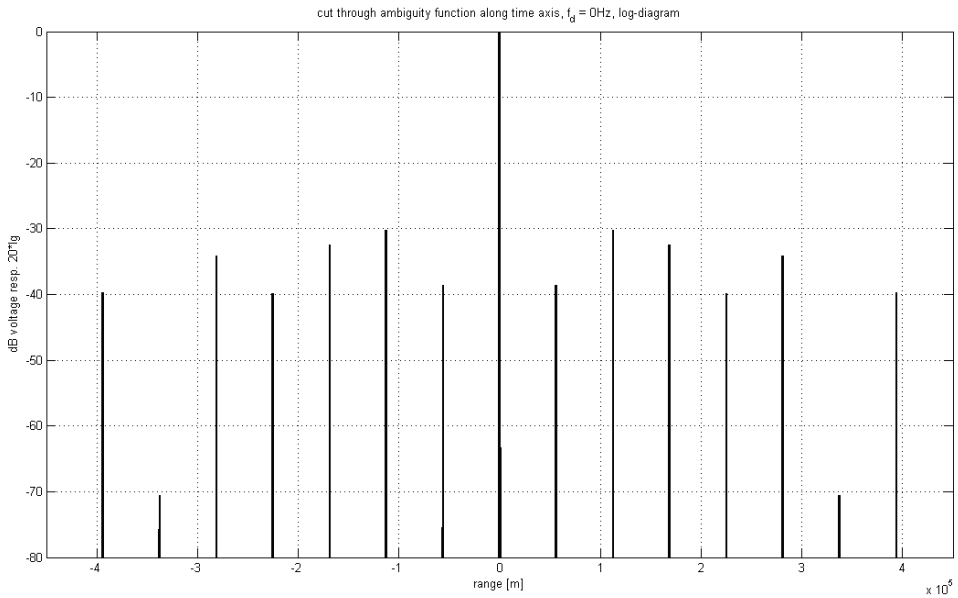

Figure 4-29 Side peak Cut of an 8-LFM-element, Barker-coded, Linear Frequency-stepped Waveform (τ_P=2µs, T_P=375µs, B=30MHz, Δf=25MHz, Barker 4⊗2)

4.6 Conclusions

After an introduction to the concept of matched filtering and the tools used for the analysis and evaluation of radar signals, signals for HRR were presented in detail.

First, frequency modulated pulses and their properties were discussed. But with respect to a surveillance radar system based on the parameters from section 1.3, all of the discussed signals suffer from limited instantaneous bandwidth, thus lacking the range resolution necessary for object classification. In addition to that, LFM and NLFM also introduce range-Doppler coupling.

In the next section phase-coded pulses were analysed. While a binary Barker-coded pulse shows a good time sidelobe level performance, it is bandwidth limited by the maximal Barker code length of N=13. The then introduced nested Barker and polyphase P4 code do not suffer from this limitation, their code length is limited only by the pulse width in combination with the sampling rate, in our chase limiting the code length to N=120 for the LPRF burst. Due to this limitation single pulses of both codes also lack the necessary range resolution for object classification.

The coherent train of identical pulses was then shown to improve Doppler resolution.

Finally, stepped-frequency waveforms were introduced as a solution to generate a high bandwidth signal when only limited instantaneous bandwidth is available. While the concept of stepped-frequency can be implemented using the MPRF as well as the LPRF burst, the lower instantaneous bandwidth in combination with the scan time needed to deliver the effective bandwidth needed lead to the analysis of SF waveforms based on the LPRF burst only. From the analyses of SF waveforms making use of different intra- and interpulse modulations it can be taken, that the necessary range resolution can be achieved by combining SF either with a LFM or P4 code. In addition to that both methods also achieve the best main peak time sidelobe levels (-49dB and -54dB, respectively). The advantage of LFM over the P4 code is that in combination with an additional interpulse modulation the overall time side peak level can be reduced significantly. This was shown for a nested Barker code and a Costas-ordered hopping sequence. With a level of -39dB the Costas-ordered interpulse modulation not only performed better then the nested Barker code (-30dB), it also has the advantage of effecting time delay and Doppler delay sidelobes in nearly the same way, as can be deduced from the properties of a single Costas-coded pulse.

5 Implementation of High Resolution in Surveillance Radar Systems

5.1 Introduction

The signals analysed in chapter 4 were based on the parameters given in section 1.3. It has been shown that a high effective signal bandwidth, and with it the necessary range resolution for object classification, can be achieved by a SF waveform, even when the available instantaneous bandwidth is limited.

The parameters itself are limited by the hardware (i.e., signal generator, mixers, D/A- and A/D-converters) available. Their values were chosen under the premises that the signals could be implemented in actual hardware without or at least only with minimal additional costs. Only for the frequency steps of the Local Oscillator (*LO*) in radar band additional logic has to be programmed for the radar processor.

Apart from the hardware limitations for HRR, which have been considered by choosing the appropriate parameters in section 1.3, other aspects in radar system design have to be considered. In section 5.2 the general aspect of SF waveforms' clutter performance is introduced, followed by necessary adoptions for SF waveform processing in a radar system's receive path and a short overview on how range profile classification influences those adoptions in section 5.3. The chapter will be closed by a summary (section 5.4).

5.2 Clutter Considerations

The detection of moving objects in the presence of clutter (see subsection 1.1.8) depends on the Signal-to-Clutter Ratio (*SCR*). So for a reliable detection the SCR has to be improved significantly. This can be achieved by minimizing the clutter entering the receiver followed by clutter cancellation (i.e., by using clutter maps). To reduce the amount of clutter entering the receiver a signal with a narrow effective pulse width can be used (Ludloff (2002)).

The Stepped-frequency Waveform (see section 4.5) is one way to combine narrow pulse width with a high signal bandwidth. The disadvantages of this waveform are object range shift as well as the spreading of the object return (Einstein (1984)), and no direct object velocity measurement.

A possible way to improve the detection of moving objects in clutter is to select the SF waveform parameters based on the induced phase shift in the received signal and relate them to the performance relevant parameters of the radar equation (Gill (1995)).

The technique of phase compensation was also picked up by Yong-Feng et al. (2006), who used what they called a Cross Stepped-frequency (*CSF*) waveform (see Figure 5-1), other then Gill (1995), who investigated a linear SF waveform. The effect of this is that the linear phase shift of the rising frequency steps compensate for the linear phase shift introduced by the falling frequency steps when the velocity error approaches zero, thus resulting in an improved radial velocity estimat. In combination with phase compensation techniques this leads to an improved SNR and subsequently to an improved SCR and moving objects detection, respectively.

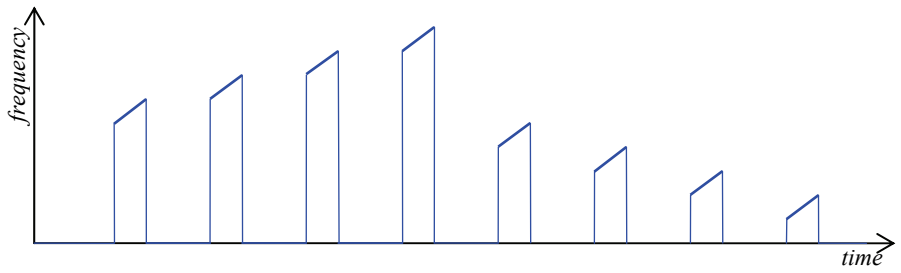

Figure 5-1 Cross Stepped-frequency Waveform of 8 LFM Pulses

As can be seen by comparing Figure 5-2 to Figure 4-18 using the CSF waveform improves the recurring side peaks level by -22dB. The range resolution is not affected by the frequency order.

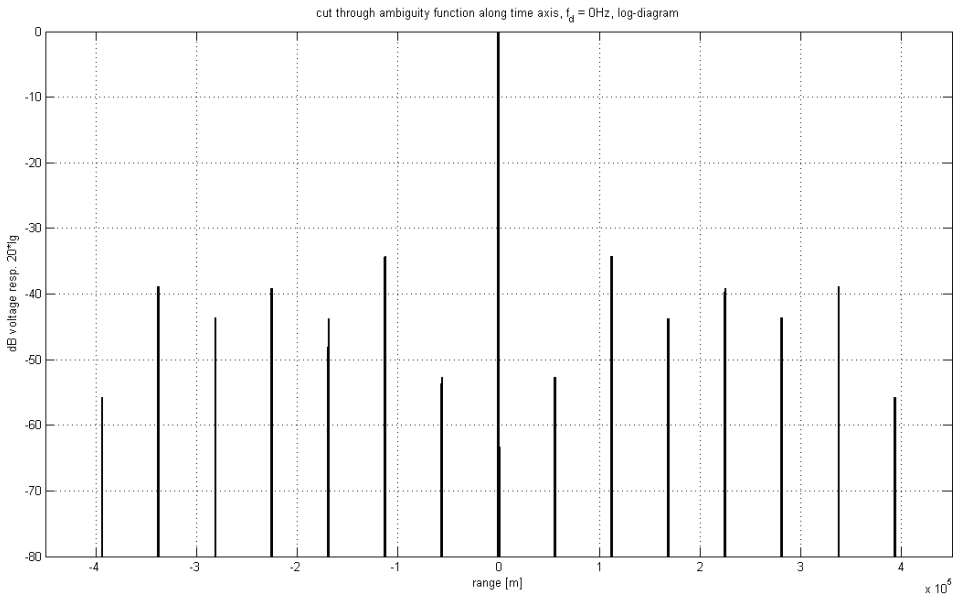

Figure 5-2 Side Peaks Cut of an 8-LFM-element Cross Stepped-frequency Waveform (τ_P=2µs, T_P=375µs, B=30MHz, Δf=25MHz)

5.3 Receive Channel

To use SF waveforms for classification three additional components are needed in the receive channel.

As the noncoherent processing of a SF waveform is performed on all pulses that contribute to the effective signal bandwidth, storage is needed for the returned signals before they can be processed. After down sampling in the receive path the digital signal has a data rate of 120 megasamples per second. For the LPRF burst analysed this means that the reflected signal of a single pulse of duration τ_P=2μs is represented by 240 samples. Each I and Q sample is stored as a 4 byte data word plus additional 100 bytes of header data. So one memory slot for the LPRF burst with 8 pulses has to be of size

$$8 \cdot \left[\left(240 \cdot 4\text{B}\right) + \left(240 \cdot 4\text{B}\right) + 100\text{B} \right] = 16160\text{B} \cong 16\text{kB}$$

and for every object that should be tracked and classified simultaneously one memory slot would be needed.

The second component needed is storage for the processed echoes before they can be processed by the pattern recognition system, the third component needed for a classification capability. These components are highly dependent on how the pattern recognition system and its attached reference database are implemented. Due to the high variability of HRR range profiles (see section 2.3) an object cannot be represented in the reference database by a single range profile.

I.e., if we want to classify an object based on an one-to-one approach (one echo is compared to one stored range profile) with range profiles of 1-degree-interval, this would mean that the reference database has to hold 360 range profiles in aspect azimuth α (0° to 359°) for one value of aspect elevation θ. If a single range profile consists of 240 sample values stored as a 4 byte data word and we also cover θ in 1-degree-intervals from -45°,…,45° if follows that for a single type of object the reference database needs a memory slot of

$$91 \cdot \left[360 \cdot \left(240 \cdot 4\text{B}\right) \right] = 31449600\text{B} \cong 30\text{MB}$$

If we want to classify, i.e., based on a three-to-one approach (the average of 3 echoes is compared to one stored range profile) it follows that the storage between matched filter and pattern recognition system needs to be big enough to store the data of 3 echoes and the average needs to be calculated. Finally the pattern recognition system also needs to be equipped with an aspect angle (see section 2.2) estimation capability.

5.4 Summary

In this chapter we addressed how the implementation of high range resolution influences the transmit channel of the radar system assumed in this thesis. Then the topic of clutter performance was introduced and a technique was presented to especially improve the performance of stepped-frequency waveforms in a clutter environment. After that an overview of receive channel components necessary for a classification capability was given.

6 Conclusions

This diploma thesis was devoted to the design and analysis of a radar signal enabling an object classification capability in surveillance radar systems based on high-resolution radar range profiles.

The analyses were performed for a surveillance radar system which parameters were assumed within the limits of radar hardware available on today's market. This limitation was necessary because research and development contribute disproportional to system's costs, especially if the production of only a small number of systems can be expected. And it eliminated the need to address the system's hardware like transmission components, mixers, antenna, or filters.

As a result of earlier research on classification of high-resolution radar range profiles the goal was to design a radar signal that would achieve an effective signal bandwidth of more then 200MHz or a range resolution of 0.75m, respectively.

The analyses of single pulse signals showed that none of the considered modulation and code types was able to achieve the desired effective bandwidth. It is unlikely that in near future there will be C-band radar hardware available that would be able to do so with a single pulse signal. That is why the concept of stepped-frequency waveforms was introduced and analysed. From the stepped-frequency waveforms considered in this thesis it can be concluded that not all modulation or code types are suitable for the assumed surveillance radar system. The combination of linear frequency intrapulse modulation and Costas-ordered stepped-frequency interpulse modulation not only achieved the desired range resolution but brings with it the advantages of being easy to implement, introducing a random-like signal component, and achieving good time sidelobe levels.

So in the assumed surveillance radar system an object classification capability can be enabled by coordinating the radar band local oscillator, as source for the Costas-ordered stepped-frequency interpulse modulation, with the direct digital synthesizer, as source for the linear frequency intrapulse modulation, via the radar processor without additional costs.

The way ahead will have to focus on the receive channel, on the pattern recognition system in particular. Independent of its implementation additional memory will be needed. Today memory for digital systems is available in many different forms as cost-efficient mass product. For that memory can be assumed to raise the costs for a classification capability only moderately.

As for the pattern recognition system itself, the way of how recorded high-resolution radar range profiles will be stored within and based on what classification algorithm/algorithms will be used will have great influence on the overall performance of object classification. It would also be interesting to see if it would be beneficiary to the signal-to-noise ration to process the effective bandwidth of two burst of the proposed radar signal and then use an additional decompression level in the support vector machine of the pattern classification system.

Based on the radar signal proposed in this thesis first test sets of high-resolution radar range profiles can be recorded for further research on the pattern recognition system.

For the radar signal additional analysis of its performance for higher Doppler would be necessary. Using a pure 64-bit simulation environment (64-bit processor, 64-bit operating system, 64-bit MATLAB®) should allow this with the desired precision. Also only the range resolution based on the matched filter's output has been analysed here. The performance on single point targets and on multiple-scatterer targets still needs investigation.

Finally the MATLAB® toolbox used for analyses has been rewritten for better memory utilization, but a complete revision was not part of this thesis. It has a few more or less minor bugs that do not influence the analyses performed for this thesis but do prevented the analysis of certain signals, e.g., Costas-coded intrapulse modulation.

In this thesis a cost-effective way was presented to enable an object classification capability in a surveillance radar system based on high-resolution radar range profiles, the use of a linear frequency intrapulse modulated, Costas-ordered stepped-frequency waveform, and available radar hardware. Further research has to be performed on the pattern classification system, additional signal fine tuning, and the reference database.

Bibliography

BBC News: *On this day, 3 July 1988 (http://news.bbc.co.uk/onthisday/low/dates/stories/july/3/newsid_4678000/4678707.stm)*. 20/05/2008. [1]

Blanz, V.; Scholkopf, B.; Bulthoff, H.; Burges, C.; Vapnik, V.N.; Vetter, T.: *Comparison of view-based object recognition algorithms using realistic 3D models*. Proc. of ICANN '96, Vol. 1112, pp. 251-256, 1996.

BMW AG: *BMW 3 Series Coupé*. Munich, Catalogue 8 11 003 027 18 1 2008 VZ, 2008.

Broomhead, D.S.; Lowe, David: *Multivariable Functional Interpolation and Adaptive Networks*. Complex Systems, Vol. 2, No. 3, pp. 321-355, 1988.

Costas, John P.: *A Study of a Class of Detection Waveforms Having Nearly Ideal Range-Doppler Ambiguity Properties*. Proc. of the IEEE, Vol. 72, No. 8, pp. 996-1009, August 1984.

Cook, Charles E.; Bernfeld, Martin: *Radar Signals: An Introduction to Theory and Application*. New York; London: Academic Press, 1967.

Duda, Richard O.; Hart, E.; Stork, David G.: *Pattern Classification*. 2nd ed.. New York: John Wiley & Sons, 2001.

Einstein, T.H.: *Generation of High Resolution Radar Range Profiles and Range Profile Auto-Correlation Functions using Stepped-Frequency Pulse Trains*. Lexington, Massachusetts Institute of Technology, Lincoln Laboratory, Project Report TT-54, October 1984.

Feixing, Wang; Yongfeng, Zhu; Hongzhong, Zhao; Qiang, Fu: *Method of Resolving the Range Ambiguity for High PRF Stepped-Frequency Radar*. Proc. of CIE '06, pp. 1-4, October 2006.

Gill, G.S.: *Step Frequency Waveform Design and Processing for Detection of Moving Targets in Clutter*. Proc. of IRC '95, pp. 573-578, May 1995.

Golomb, Solomon W.; Taylor, Herbert: *Construction and Properties of Costas Arrays*. Proc. of the IEEE, Vol. 72, No. 9, pp. 1143-1163, September 1984.

[1] Documents marked with come on CD-ROM with this thesis.

Harris, Fredric J.: *On the use of windows for harmonic analysis with the discrete Fourier transform*. Proc. of the IEEE, Vol. 66, No. 1, pp. 51-83, January 1978.

IEEE Std 521-2002. *IEEE Standard for Letter Designations for Radar-Frequency Bands*.

IEEE Std 686-2008. *IEEE Standard Radar Definitions*.

Jacobson, Nathan: *Basic Algebra I*. 2nd ed.. New York: W.H. Freeman, 1985.

Joachims, Thorsten: *Text Categorization with Support Vector Machines: Learning with Many Relevant Features*. Rev. ed.. Dortmund, University, Computer Science Department, LS-8 Report 23, April 1998.

Kastinger, Christian: *Capability of Support Vector Machines for Automatic Target Classification of Simulated Radar Range Profiles*. Klagenfurt, University of Applied Sciences, Carinthia Tech Institute, Master Thesis, 2006.

Knott, Eugene F.; Shaeffer, John F.; Tuley, Michael T.: *Radar Cross Section*. 2nd ed.. Boston; London: Artech House, 1993.

Kretschmer, Frank F.; Lewis Bernard L.: *Doppler Properties of Polyphase Coded Pulse Compression Waveforms*. IEEE Trans. Aerospace and Electronic Systems, Vol. AES-19, No. 4, pp. 521-531, July 1983.

Levanon, Nadav; Mozeson, Eli: *Radar Signals*. New York: John Wiley & Sons, 2004.

Lewis, Bernard L.; Kretschmer, Frank F.: *Linear Frequency Modulation Derived Polyphase Pulse Compression Codes*. IEEE Trans. Aerospace and Electronic Systems, Vol. AES-18, No. 5, pp. 637-641, September 1982.

Ludloff, Albrecht: *Praxiswissen Radar und Radarsignalverarbeitung*. 3rd ed.. Braunschweig; Wiesbaden: Vieweg, 2002.

Mahafza, Bassem R.: *Radar Systems Analysis and Design Using MATLAB*. 2nd ed.. Boca Raton: Chapman & Hall/CRC, 2005.

Mallat, Stéphane: *A Wavelet Tour of Signal Processing*. 2nd ed.. San Diego: Academic Press, 1999.

Markowetz, Florian: *Klassifikation mit Support Vector Machines*. Berlin, Centre for Genome Based Bioinformatics, Genomische Datenanalyse 2003, 2003.

Mathworks, The: *Tech Note 1107 - Avoiding Out of Memory Errors (http://www.mathworks.com/support/tech-notes/1100/1107.html)*. 27/07/2008.

Meier, Sabine: *Radarverfahren zur Optimierung der Entfernungsauflösung*. Berlin, University of Applied Sciences, Department of Engineering Sciences 1, Diploma Thesis, 2007.

Paulose, Abraham T.: *High Range Resolution with the Step Frequency Waveform*. Monterey, Naval Postgraduate School, Master Thesis, 1994

Prodi, Francesco; Tilli, Enrico: *Motion Compensation for a Frequency Stepped Radar*. Waveform Diversity and Design, pp. 255-259, June 2007

Raytheon Company: *The Standard Missile Family (http://www.raytheon.com/capabilities/products/standard_missile/)*. 20/05/2008.

Rihaczek, August W.: *Principles of High-Resolution Radar*. Boston; London: Artech House, 1996.

Ruttenberg, Kenneth; Chanzit, Lawrence: *High Range Resolution by Means of Pulse-to-Pulse Frequency Shifting*. Proc. of EASCON '68, pp. 47-51, 1968

Schölkopf, Bernhard; Smola, Alexander J.: *Learning with Kernels: Support Vector Machines, Regularization, Optimization, and Beyond*. Cambridge, MA: MIT Press, 2001.

Sinsky, A.I.;Wang, C.P.: *Standardization of the Definition of the Radar Ambiguity Function*. IEEE Trans. Aerospace and Electronic Systems, Vol. AES-10, No. 4, pp. 532-533, July 1974.

Skolnik, Merrill I.: *Introduction to Radar Systems*. 3rd ed.. New York; Chicago: McGraw Hill, 2001.

Skolnik, Merrill I.: *Radar Handbook*. 3rd ed.. New York; Chicago: McGraw Hill, 2008.

Stimson,George W.: *Introduction to Airborne Radar*. 2nd ed.. El Segundo: Hughes Aircraft, 1998.

Temple, M.A.; Sitler, K.L.; Raines, R.A.; Hughes, J.A.: *High range resolution (HRR) improvement using synthetic HRR processing and stepped-frequency polyphase coding*. Proc. of Radar, Sonar and Navigation, Vol. 151, No. 1, pp. 41-47, February 2004.

Tsujinishi, Daisuke; Koshiba, Yoshiaki; Abe, Shigeo: *Why Pairwise Is Better then One-against-All or All-at-Once*. Proc. of Neural Networks '04, Vol. 1, pp. 698-701, July 2004.

Unterberg, W.: *Simulation der automatischen Analyse von Radarbildern*. Ulm, University of Applied Sciences, Diploma thesis, 2005.

van der Heiden, René; de Vries, J.: *The ORFEO measurement campaign*. The Hague, TNO Defence Research, TNO Physics and Electronics Laboratory, FEL-96-A073, August 1996.

van der Heiden, René: *Aircraft Recognition with Radar Range Profiles*. Amsterdam, University, Faculty of Science, Dissertation, 1998.

Vapnik, V.; Lerner, A.: *Pattern recognition using generalized portrait method*. Automation and Remote Control, Vol. 24, pp. 774-780, 1963.

Wehner, Donald R.: *High-Resolution Radar*. 2nd ed.. Boston; London: Artech House, 1995.

Woodward, Philip M.: *Probability and Information Theory with Application to Radar*. Oxford: Pergamon Press, 1953.

Yong-Feng, Zhu; Hong-Zhong, Zhao; Qiang, Fu: *Simultaneously Velocity Measuring and HRR Profiling with a Novel CSF Sequence*. Proc. of CIE '06, pp. 1-5, October 2006.

Zwart, Joris P.: *Aircraft Recognition from Features Extracted from Measured and Simulated Radar Range Profiles*. Amsterdam, University, Faculty of Science, Dissertation, 2003.

List of Tables

List of Figures

Symbols

A_e	Effective Antenna Aperture
B	Bandwidth
B_I	Instantaneous Bandwidth
B_{SF}	Stepped-frequency Waveform Bandwidth
BT	Time-Bandwidth Product
c	Speed of Light
E_i	Incident Electric RF Field
E_s	Backscattered Electric RF Field
f_0	Carrier Frequency / Centre Frequency / Radio Frequency
f_d	Doppler Frequency Shift
f_i	Centre Frequency of the i-th (Sub-)Pulse/Bit
f_R	Frequency of Received Signal
G	Gain
M	Integer
N	Integer
$\mathbf{N}$	Set of Natural Numbers (excl. Zero)
P_{Tx}	Transmitted Power
$p(\mathbf{x}\|m)$	Class-Conditional Probability
$P(m)$	Probability for a State of Nature m
$P(m\|\mathbf{x})$	A Posteriori Probability
R	Distance between Radar System and Object
R_{max}	Maximum Detection Range
S_{min}	Minimum Detectable Signal
t_b	Subpulse/Bit Width
T	Pulse Duration / Pulse Width
T_P	Pulse Repetition Interval
T_R	Time Delay between Transmitted and Received Signal
T_S	Sampling Rate
$u(t)$	Complex Envelop of Signal

v	Velocity
v_R	Radial Velocity
v_T	Tangential Velocity
$\mathbf{x}$	Feature Vector
α	Aspect Azimuth
$\chi(\tau, \vartheta)$	Woodward's (Auto-)Correlation Function
$\lvert\chi(\tau, f_d)\rvert^2$	Ambiguity Function
λ	Wavelength
θ	Aspect Elevation
σ	Radar Cross Section
τ	Range Delay
τ_P	Pulse Width
Δf	Frequency Step
ΔR	Range Resolution

A Flight IR655

ON THIS DAY 3 July

Graphics version >> BBC News >>

Search ON THIS DAY by date 3 July

Front Page | Years | Themes | Witness

1988: US warship shoots down Iranian airliner

An American naval warship patrolling in the Persian Gulf has shot down an Iranian passenger jet after apparently mistaking it for an F-14 fighter.
All those on board the airliner - almost 300 people - are believed dead.
The plane, an Airbus A300, was making a routine flight from Bandar Abbas, in Iran, to Dubai in the United Arab Emirates.
The USS Vincennes had tracked the plane electronically and warned it to keep away. When it did not the ship fired two surface-to-air missiles, at least one of which hit the airliner.
Navy officials said the Vincennes' crew believed they were firing at an Iranian F14 jet fighter, although they had not confirmed this visually.

No survivors

The plane blew up six miles from the Vincennes, the wreckage falling in Iranian territorial waters.
Iranian ships and helicopters have been searching for survivors but none have so far been found.
Iranian television broadcast scenes of bodies floating amid scattered debris.
Iran has reacted with outrage, accusing the United States of a "barbaric massacre" and vowed to "avenge the blood of our martyrs".
President Reagan said the Vincennes had taken "a proper defensive action" and called the incident an "understandable accident", although he said he regretted the loss of life.

'Deep regret'

Admiral William J Crowe, Jr, chairman of the Joint Chiefs of Staff, said at a Pentagon news conference that the US government deeply regretted the incident.
However, he said, the Airbus was four miles west of the usual commercial airline route and the pilot ignored repeated radio warnings from the Vincennes to change course.
Less than an hour before the shooting down of the passenger jet, he added, the Vincennes was engaged in a gun battle with three Iranian gunboats after a helicopter from the Vincennes was fired on.
The president promised a full investigation into how a passenger jet came to be mistaken for a fighter jet, which is two-thirds smaller.
US warships have been escorting Kuwaiti tankers in and out of the Persian Gulf since last July as part of its controversial undertaking to keep the Straits of Hormuz open during the eight-year-old Iran-Iraq War.

Pentagon officials acknowledged at the time that increased US military presence would risk provoking confrontations with Iran.
Last May the patrol frigate USS Stark was almost sunk by an Iraqi fighter-bomber, killing 37 sailors. Vigilance was tightened after the incident.

In Context

Most of those on board the Iranian Airbus were Iranians on their way to Mecca. The victims also included 66 children and 38 foreign nationals.
An official inquiry carried out by the US attributed the mistake to human error.
However, the Iranian government has always disputed the American version of events.
It took four years for the US administration to admit officially that the USS Vincennes was in Iranian waters when the skirmish took place with the Iranian gunboats.
Subsequent investigations have accused the US military of waging a covert war against Iran in support of Iraq.
The US government has never admitted responsibility or apologised for the tragedy.
Some believe the Lockerbie bombing, carried out six months later in December 1988, was masterminded by Iranians in revenge for the Airbus tragedy, although a Libyan man was convicted and jailed in 2001.
In February 1996 the US agreed to pay Iran $61.8 million in compensation for the 248 Iranians killed, plus the cost of the aircraft and legal expenses.
It had already paid a further $40 million to the other countries whose nationals were killed.

Search ON THIS DAY by date 3 July

Front Page | Years | Themes | Witness

^^ Back to top | ©

B SM-2

Enter keyw ord Search

Home > Capabilities > Products and Capabilities > Standard Missile

The Standard Missile Family

Standard Missile is the world's choice for air defense and theater ballistic missile defense. For 50 years, Standard Missile technology has evolved to keep pace with the threat and grow into new missions. Standard was developed as a replacement for the Terrier, Talos and Tartar surface-to-air missiles.

SM-1 entered production in 1967 and remains in operation with many international navies. Raytheon has assumed support of SM-1 and is leading a team of companies to provide users around the globe with access to spares and repair services.

SM-2's primary role is to provide area defense against enemy aircraft and anti-ship cruise missiles. SM-2 is deployed in several configurations, ranging from SM-2 Block IIIA to SM-2 Block IV Extended Range.

SM-3 is being developed as part of the Missile Defense Agency's sea-based Aegis Ballistic Missile Defense System. The missiles will be deployed on Aegis cruisers and destroyers to defend against short- to intermediate-range ballistic missile threats in the midcourse phase of flight. Raytheon also is developing the Kinetic Warhead for SM-3.

SM-6, Extended Range Active Missile, is being developed to meet the Navy's requirement for an extended range anti-air warfare (ER-AAW) missile. The initial program will provide capability against fixed and rotary wing aircraft, unmanned aerial vehicles and land attack anti-ship cruise missiles in flight, both over sea and land. With a future integrated fire control, SM-6 will provide the surface Navy with an increased battlespace against over-the-horizon AAW threats, taking full advantage of the kinematics available to Standard Missile. SM-6 will employ the SM-2 Block IV airframe and proven seeker and guidance technology from across the company's product lines.

Downloads

SM-1

SM-2

SM-3

SM-6

John Farlow
Media Relations
Raytheon Company
1151 E Hermans Rd
Tucson, AZ 85706
Phone: (520)794-1211
Fax: (520)794-2899
mailto:John_A_Farlow@raytheon.com

C CD-ROM Content

/matlab

./toolbox_kothe contains the rewritten MATLAB® toolbox as M-files.

./waveforms contains subfolders labelled (***a***b_***b***p_***c***-***d***e***e***_***f***(***g***)_sf(***h***)) according to the signal analysis stored within. The information included in the folder name is

- ***a*** the number of bursts (b),
- ***b*** the number of pulses (p) per burst,
- ***c*** the PRI and
- ***d*** the pulse width
- ***e*** in seconds expressed in the exponential format (e),
- ***f*** the intrapulse modulation

bark	binary Barker code (subsection 4.3.1)
lfmu	Linear Frequency Modulation (subsection 4.2.1), Up-chirp
nlfm	Nonlinear Frequency Modulation (subsection 4.2.2)
p4	Polyphase P4 code (subsection 4.3.3)
rect	Unmodulated / rectangular Pulse

with

- ***g*** the bandwidth (in MHz) / code length used, and
- ***h*** the interpulse modulation

bark2x4	Nested 2⊗4 Barker Code
bark4x2	Nested 4⊗2 Barker Code
cost25	Costas-ordered Stepped-frequency (Δf=25MHz)
cross25	Cross Stepped-frequency (Δf=25MHz)
lu15	Linear Stepped-frequency (Δf=15MHz)
lu25	Linear Stepped-frequency (Δf=25MHz)
lu30	Linear Stepped-frequency (Δf=30MHz)

with the frequency step / code length used for the stepped-frequency (sf) waveform.

I.e., the label `1b_8p_375-2e-6_lfmu(30)_sf(lu25+bark2x4)` refers to one burst of 8 pulses, a PRI of 375µs, and a pulse width of 2µs, where the single pulses are Up-chirps with an instantaneous bandwidth of 30MHz and the burst is a linear Up-stepped-frequency waveform with the single frequency steps itself modulated as a nested 2⊗4 Barker code.

`./ab_bp_c-dee_f(g)_sf(h)` contains the full time axis plot at zero Doppler (`cut_time_axis.fig`), its main peak (`sidelobe_level_main_peak.png`) and side peaks (`sidelobe_level_side_peaks.png`) details, the definition files used for the analysis (`Define_Inputdata_Additional.m`, `Define_Inputdata_Signalwaveform.m`), and the workspace content at the end of the main program (`workspace.mat`), for each analysed signal.

`./toolbox_meier` contains the MATLAB® toolbox from Meier (2007) introduced in subsection 4.1.3.

`./beispieldateien`

`./Beispiel0` contains the definition files for a train of 5 rectangular pulses.

`./Beispiel1` contains the definition files for single rectangular pulse.

`./Beispiel2` contains the definition files for a single LFM pulse.

`./Datapool` contains the definition file for an external signal (`extern_file.txt`) and, if selected, the saved signal (`timerow.mat`).

/presentations contains the mid-term (`2008-04-24_mid-term.ppt`) and end-term (`2008-04-24_mid-term.ppt`) PowerPoint® presentations to this thesis, held at EADS Deutschland GmbH.

/thesis contains the PDF-document of this thesis.

`./bibliography` contains the PDF-files of the documents marked by in the Bibliography.

`./figures`

`./appendix` contains the symbol used in the Bibliography to mark documents that come on CD-ROM with this thesis.

`./chapter_2`	contains certain figures presented in chapter 2 as JPG- and PNG-files. The files are named according to their label text.
`./chapter_4`	contains certain figures presented in chapter 4 as JPG- and PNG-files. The files are named according to their label text.
`./chapter_5`	contains certain figures presented in chapter 5 as PNG-files. The files are named according to their label text.
`./preface`	contains the EADS Defence & Security figures used on the title page.